Politecnico di Torino

POLITECNICO DI TORINO

MASTER OF SCIENCE IN COMMUNICATIONS AND COMPUTER NETWORKS ENGINEERING

Surface damage assessment by analysis of electrical resistance changes

Academic Advisor:

Supervisor: Prof. Ladislau MATEKOVITS

PhD. Eng. Mihai Iulian,

National Metrology Institute of Italy, INRiM

Candidate:

Taimoor Javed (S290022)

FEBURARY 2024

TABLE OF CONTENT

Acronyms and Notations

SEM	Scanning Electron Microscopy
RHEED	Reflection-High-Energy Electron Diffraction
SREM	Scanning Reflection Electron Microscopy
MT	Moiré Technique
CSMGFRP	Chopped Strand Mat Glass Fiber Reinforced Polyester
ANOVA	Analysis Of Variance
MPa	Mega Pascals
DC	Direct Current
V	Electrical Potential Difference
I	Electric Current
R	Electrical Resistance
A	Ampere
ohm-m	Resistivity
S/m	Electrical Conductivity

Acknowledgment

I express my deepest appreciation to Prof. Ladislau Matekovits, my dedicated supervisor, for his unwavering support and mentorship during my doctoral research. His wealth of knowledge, insightful guidance, and constructive feedback have been instrumental in shaping the trajectory of my academic endeavors. I am also grateful to Dr. Mihai Iulian, PhD. Eng., from the National Metrology Institute of Italy (INRiM), whose expertise and collaboration enriched my research experience. His contributions and thoughtful insights have added depth and precision to my work. INRiM provided an exceptional research environment, and I extend my thanks to the institution for granting me access to resources and facilities crucial for the success of my project.

ABSTRACT

This research presents a comprehensive investigation into the assessment of surface damage in Ti-3Al-2.5V alloy, a near-alpha, alpha-beta alloy widely used in aerospace and medical applications. The study adopts a multifaceted approach, integrating real-world data collection, simulated scenarios, and advanced data analysis techniques to enhance the understanding of surface degradation in this crucial material. The introduction outlines the significance of evaluating surface damage in materials like Ti-3Al-2.5V, emphasizing its applications in aircraft components, medical implants, and other critical sectors. The chapter sets the stage for the subsequent discussions, highlighting the importance of assessing surface damage for structural integrity and functionality. This chapter details the methodology employed in the study, encompassing data collection, analysis, and presentation of results. The four-point probe method is selected for its efficacy in measuring resistivity in small specimens, with a specific focus on Ti-3Al-2.5V. Scilab is introduced as a versatile tool for data processing and visualization. The section on data simulation reveals the innovative use of fictitious datasets to validate research methods, acknowledging the assumptions inherent in data modeling. The chapter concludes by highlighting the synergistic relationship between real-world data collection and data modeling in achieving a robust surface damage assessment. The heart of the research lies in this chapter, where a multifaceted exploration of surface damage in Ti-3Al-2.5V is presented. Outlier detection and calibration methods are employed to ensure the integrity of collected data, addressing measurement errors and external influences. Temperature-induced surface damage simulation, mechanical stress effects, and Scilab-simulated damage patterns offer a comprehensive understanding of how varying conditions impact the electrical resistance of Ti-3Al-2.5V. The chapter integrates graphical representations, such as line plots and 3D surface plots, to visually illustrate trends, correlations, and dynamic changes over time. A particular focus on anisotropic electrical resistance distribution sheds light on the directional dependence of electrical properties in Ti-3Al-2.5V.

Keywords: Ti-3Al-2.5V alloy, surface damage assessment, electrical resistance testing, four-point- probe method, Scilab, simulated scenarios, anisotropic distribution, multifaceted approach.

CHAPTER # 1

INTRODUCTION

1.1 Background:

When assessing the structural integrity of materials for use in infrastructure, industrial settings, or research applications, surface damage evaluation is an essential component (Spencer Jr et al., 2019, Argyroudis et al., 2020). Numerous things, including mechanical stress, the climate, and aging-related wear and tear, can cause surface damage (Sarıkaya et al., 2021, Thakur and Gangopadhyay, 2016). Maintaining the dependability and safety of materials requires the ability to recognize and comprehend the level of surface deterioration (Cavaco et al., 2017). One useful metric to evaluate surface deterioration is electrical resistance (Florkowski and Kuniewski, 2023). Potential problems can be understood from the relationship between a material's electrical characteristics and structural state (Harrison, 2012). Changes in a material's microstructure, composition, or general integrity might impact its electrical conductivity when it experiences surface damage (Liao et al., 2021, La Monaca et al., 2021). By keeping an eye on variations in electrical resistance, one can identify damage early on, preventing catastrophic failures and providing preventive maintenance (Maharaj et al., 2009).

A variety of instruments, each suited to a particular set of requirements and circumstances, are used to measure electrical resistance precisely. Resistance meters, millimeters, and specialized tools like the four-point probe system are a few examples of common instruments (Kikken and Vandalon, 2018). With the use of these instruments, engineers and researchers can measure resistance precisely, which helps determine the condition of the material (Gricius, 2022). Particularly noteworthy is the four-point probe method's capacity to reduce contact resistance-related errors and produce more accurate data (Flaga et al., 2023). Software programs such as Scilab are frequently used in conjunction with the four-point probe approach to improve resistance measuring accuracy and efficiency. An open-source numerical computing platform called Scilab makes it easier to analyze and visualize scientific data. Researchers and engineers working in materials science and surface damage assessment favor it because of its vast utility and versatility (Sensi, 2019). The efficiency of the four-point probe method using Scilab is influenced by a few factors (Kreiml et al., 2021). The investigation of titanium alloys within the purview of the study lends additional significance, considering their pervasive application in vital industries.

First of all, Scilab has an intuitive user interface that makes it suitable for both novice and expert users. This feature makes sure that researchers can use the program effectively, which lowers the learning curve that comes with using sophisticated measuring methodologies. Furthermore, Scilab facilitates data

visualization, which enables users to properly analyze resistance measures. Patterns and trends related to surface deterioration can be found with the help of graphical representations of resistance changes over time or under different conditions (Fan et al., 2021, Pandiyan, 2017). Furthermore, Scilab's ability to work with a variety of data formats improves its ability to integrate with diverse measuring tools (Bunks et al., 2012). Because of its adaptability, researchers can easily input data from a variety of sources, making it easier to conduct a thorough investigation of how changes in electrical resistance affect materials that are experiencing surface damage. The scripting features of the software enable users to streamline the data collection and analysis process by automating repetitive processes.

1.2 Motivation:

The importance of this research in maintaining structural integrity in a variety of applications is the driving force for the exploration of it. Early indications of surface damage can be found by knowing the relationship between a material's electrical characteristics and its structural state. This knowledge aids in proactive maintenance strategies and the avoidance of catastrophic failures. The overall objective of improving safety and dependability in material applications is in line with this strategy. The title has a number of benefits, such as early detection, thorough content assessment, and adaptability to other sectors. In order to ensure accuracy and efficiency in resistance measurements, the four-point probe method minimizes contact resistance mistakes, which adds to the effectiveness of this approach. The approach gains versatility in data format compatibility, support for data visualization, and an easy-to-use interface when combined with Scilab. Scilab's scripting features enable users to automate processes and streamline the process of gathering and analyzing data. When taken as a whole, these components offer a strong framework for improving surface damage assessment, encouraging early identification, thorough analysis, and effective data interpretation in the interest of material safety and reliability. The study's ultimate objective is its capacity to provide specific advice for preserving the structural integrity and dependability of a titanium alloy.

1.3 Scope:

The purpose of this work is to use accurate electrical resistance measurements to do a thorough examination of surface damage in titanium alloys. This discovery is extremely relevant since titanium alloys are widely employed in industrial, medicinal, and aerospace applications. The four-point probe method, which is well-known for its precision in reducing mistakes related to contact resistance, will be employed in this study to gather exact data on the electrical resistance of titanium alloy. The inquiry will cover a range of elements, including wear and tear over time, mechanical stress, and temperature, that contribute to surface deterioration. The focus of this work is on titanium alloy in an attempt to shed light on the unique problems and traits related to surface degradation in these materials. To improve the interpretation of resistance

measurements, the integration of Scilab for data processing and visualization will also be investigated. Targeted advice for preserving titanium alloys' structural integrity and dependability in crucial applications may come from this concentrated study.

1.4 Aim:

By using the four-point probe method and Scilab analysis to perform accurate electrical resistance measurements, to further understanding of surface damage in titanium alloys.

Objectives:

- Describe the several forms of surface degradation that wear, the mechanical stress can cause in titanium alloy.
- Clearly identify the relationship between changes in electrical resistance and particular surface damage manifestations in titanium alloy.
- Examine the precision and dependability of the four-point probe method for electrical resistance measurement, paying particular attention to contact resistance error minimization.
- Examine how Scilab can be used to improve the interpretation of resistance measurements in order to spot trends and patterns related to surface damage.
- Pay close attention to the particular difficulties and traits associated with surface damage in titanium alloy under various stressors and environmental circumstances.
- Contribute to the broader field of surface damage assessment by advancing methodologies for early detection and comprehensive analysis in materials science.

1.5 Expected outcomes:

A titanium alloy in the Scilab simulations will be created with distinct damage patterns in an elliptical shape. Through the use of Scilab programs, various damage types can be created on the coated surface, emulating situations such as scraping off a portion in the middle of the plate that is around 5 mm in size. A graphical depiction of the dynamic variations in electrical surface resistivity with respect to the intact standard coated surface will be provided. This special arrangement guarantees a thorough investigation of different damage configurations, offering a refined comprehension of how different types of surface degradation affect the material's electrical characteristics. The particular results of this study should include visually striking illustrations, produced by Scilab simulations that demonstrate how different damage patterns on protective

coatings alter electrical surface resistivity. The goal of the research is to provide a thorough examination of localized differences in resistivity, as well as quantitative information on the effects of particular damage configurations, like scraping off a particular area in the middle of the coating.

1.6 Structure of Thesis:

Chapter 1: Introduction

We established the scene in this chapter by outlining the importance of evaluating surface degradation and the application of electrical resistance as a signal. We justify the use of Scilab simulations and explain how they can be used to clarify the connection between surface degradation and changes in electrical resistance. In addition, we provide the goals with a focus on integrating machine learning techniques to improve surface deterioration detection.

Chapter 2: Literature Review

The limitations of conventional surface damage assessment methods are reviewed in this section, opening the door for the incorporation of more sophisticated methodologies. We examine Scilab's current uses in materials science, highlighting its contribution to the simulation of changes in electrical resistance caused by surface degradation. We also review the literature on using machine learning to detect damage, emphasizing how applicable these methods are to our research.

Chapter 3: Methodology

We describe the process in detail and show how to build up simulations with Scilab to produce a measuring matrix that reflects variations in surface damage. In parallel, we present the experimental setup for physical measurements that yield a similar matrix using either Four Point Probes or Two Point Probes. The chapter also describes how these matrices will be analyzed and surface deterioration will be successfully detected by integrating machine learning techniques.

Chapter 4: Findings and Interpretation

The results of Scilab simulations are shown in this chapter along with an analysis of the relationship between surface damage and the measurement matrix that was developed. We examine the matrix derived from empirical measurements, highlighting the contrast with synthetic data. We also provide the outcomes of using machine learning techniques to identify surface degradation using the matrices, emphasizing the usefulness of the combined method.

Chapter 5: Conclusion and Suggestions

This chapter concludes the thesis by providing suggestions for the integrated approach's practical use in real-world situations. We talk about the usefulness of applying machine learning and Scilab simulations to improve surface damage assessment. Limitations are addressed, research directions are suggested, and the significance of our results for the advancement of surface damage detection is emphasized.

CHAPTER # 2

Literature Review

The assessment of surface damage in materials is a critical aspect of ensuring structural integrity across various applications. This literature review explores existing methodologies with a focus on electrical resistance-based approaches and delves into studies utilizing the four-point probe method for similar purposes. While the four-point probe method proves effective, challenges such as contact resistance and calibration issues persist. Moreover, the literature lacks comprehensive analyses of specific materials, such as titanium alloys, under various stressors. The use of Scilab introduces computational efficiencies but requires careful consideration of data input and interpretation.

2.1 Electrical Resistance-Based Approaches:

Early research by established the correlation between a material's electrical characteristics and its structural state, emphasizing electrical resistance as a key metric for surface damage evaluation. Further supported this, noting that variations in microstructure, composition, or overall integrity impact electrical conductivity during surface damage. To measure electrical resistance, various models and methods have been proposed. Contact resistance and sample shape, i.e. whether it is in the form of a single crystal, thin film, powder pellet, or small crystallite, are factors influencing the applicability of various procedures and the precision attained. Two probes (ohmmeter or voltmeter ammeter measurements) can be used for greater resistive samples, while four probes (potential probe measurements) can be used for low resistive and single crystals (Lovisari et al., 2010). Montgomery, van der Pauw, and Smith methods are used for pellets and bulky samples. The use of resistivity measurement in scientific activity is not new, and there are numerous excellent accounts of various measuring techniques accessible."

2.1.1 Two probes measurements:

This method is effective when the sample has a high resistance. Figure 2.1 depicts the simplest way of measuring resistivity (See and Deng, 2004). The voltage drop V across the sample and current through the sample I are measured using this method. The resistivity is then expressed as follows:

$$\rho = \frac{VA}{IL} \tag{1}$$

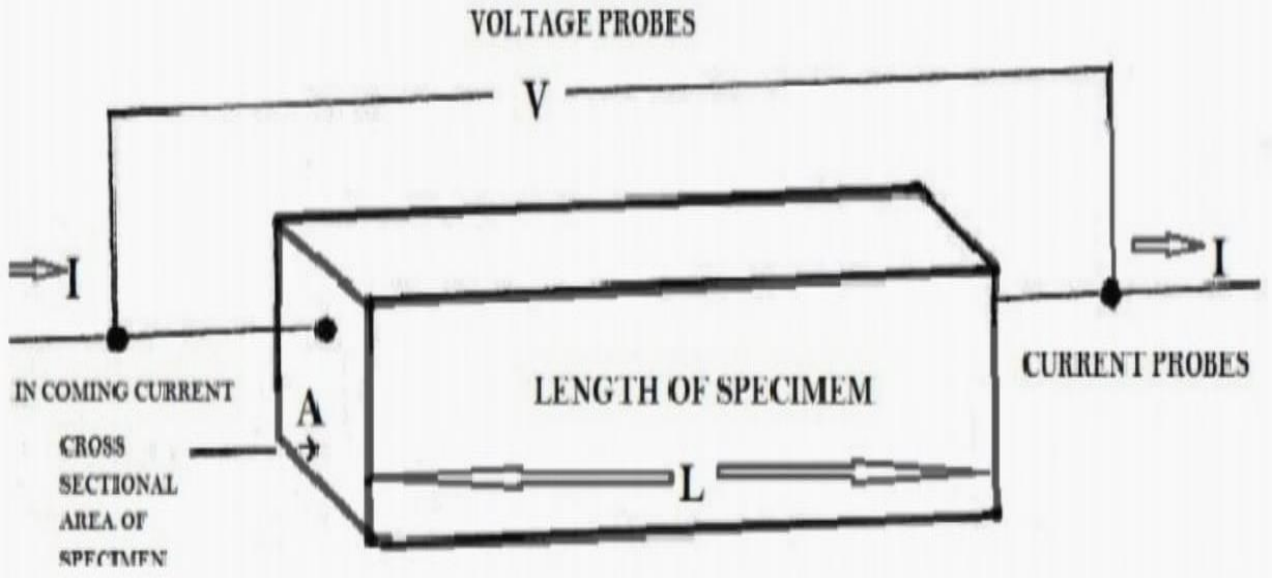

Figure 2.1: Measuring electrical resistance using two probes

2.1.2 Four probes measurements:

The most used technique for measuring resistivity on low resistive samples is the potential probe. This method substitutes the distance D between the two probes for the sample length L in equation (1) by measuring the potential drop across the two probes. The distance between the centres, not the closest distance between the probes, is the most accurate value for the probe distance in the event that the probes are not point contacts. The method's schematic arrangement is depicted in Figure 2.2. Here, p is provided by:

$$\rho = \frac{V_D A}{DI} \tag{2}$$

The resistance of both the bulk specimen and the single crystal can be measured using the four probe approach (Mavrokefalos et al., 2007, Miccoli et al., 2015). Here, current flows through the outer contacts that are in close proximity to the sample's margins. The inner contacts' potential difference is measured. This technique works well for low and precise resistance measurements because it can remove the effects of contact resistance between the sample and electrical connections.

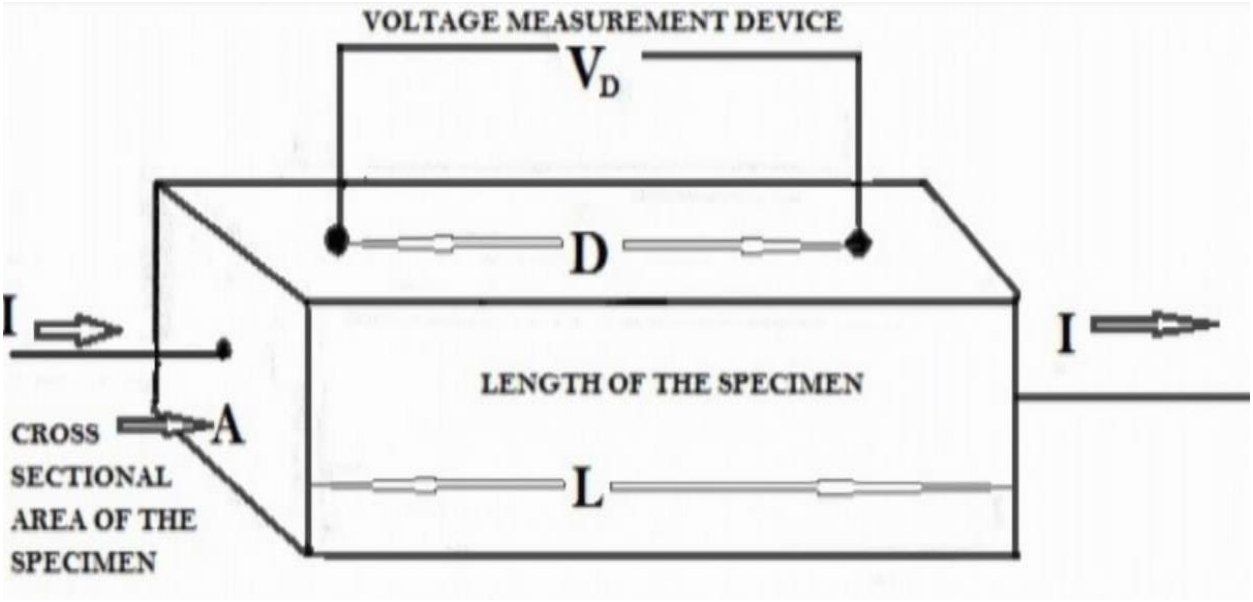

Figure 2.2: Measurement of electrical resistivity with four probes

The four point approach cancels out contact and lead resistances, but if these generate enough heat, contact resistance can still result in errors. Low resistance in the connections is therefore essential. The issue is also caused by instrumental de offsets, but this is readily fixed by subtracting. The mistake is exacerbated by self-induced voltage offsets in the circuit. Reversing the current flow through the sample will solve this issue. Signal noise also increases the error when the low level of voltage (in the range of μV) is produced across the sample. Noise issues can be lessened by utilizing low heat contactors and the appropriate shielded wires, as well as single point grounding.

2.1.3 Resistivity measurement for a disc of arbitrary shape (Pauw Method)

Vander Pauw presents this technique for measuring the resistivity of a flat disc (pellet) of any shape without having to know the current pattern. This technique is only useful if the following criteria are met:

A. The contacts are located around the sample's perimeter.

B. The contacts are just the right size.

C. The thickness of the sample is uniform.

D. The sample's surface is singly connected, meaning it lacks isolated holes. As illustrated in Figure 2.3, a sample with an arbitrary shape and relatively low resistance satisfies all conditions (A) through (D).

The potential difference VD - VC between D and C contacts per unit current through the contacts A and B is the definition of the resistance RABCD. In this instance, contact A allows current to enter the sample, and contact B allows it to exit. RBCDA resistance is described in a similar way. The resistivity of a sample with a uniform thickness "d" is determined by its RAB, CD, RBC, DA, and'd'. With a few restrictions, this method can be very helpful in determining the electrical resistivity of materials of any shape, but it has also been changed by other scientists. Ronald Chwang et al. looked at how finite size contacts with particular shapes affected the measurement of Hall coefficient and van der Pauw's resistivity on a square sample. Correction factors for the apparent observed values at zero magnetic fields were derived from computerized over-relaxation calculations and electrolytic tank experiments for the sheet resistivity measurement. Using a fast-convergent over-relaxation technique, correction factors were derived for the Hall coefficient for the effects of voltage shorting caused by current electrodes and current shorting caused by Hall electrodes throughout a range of Hall angles, tan 0 = 0.1-0.5. Using an electrolytic tank, the current shorting contribution to the correction factor at zero magnetic field was also precisely determined (Szymański et al., 2015, Nahlik et al., 2011). The Hall errors caused by the voltage and current electrodes were roughly equal in the symmetrical configurations under study. The research demonstrates that a reasonable approximation to van der Pauw's infinitesimal contact can be made using contacts that are sizable in comparison to the sample size.

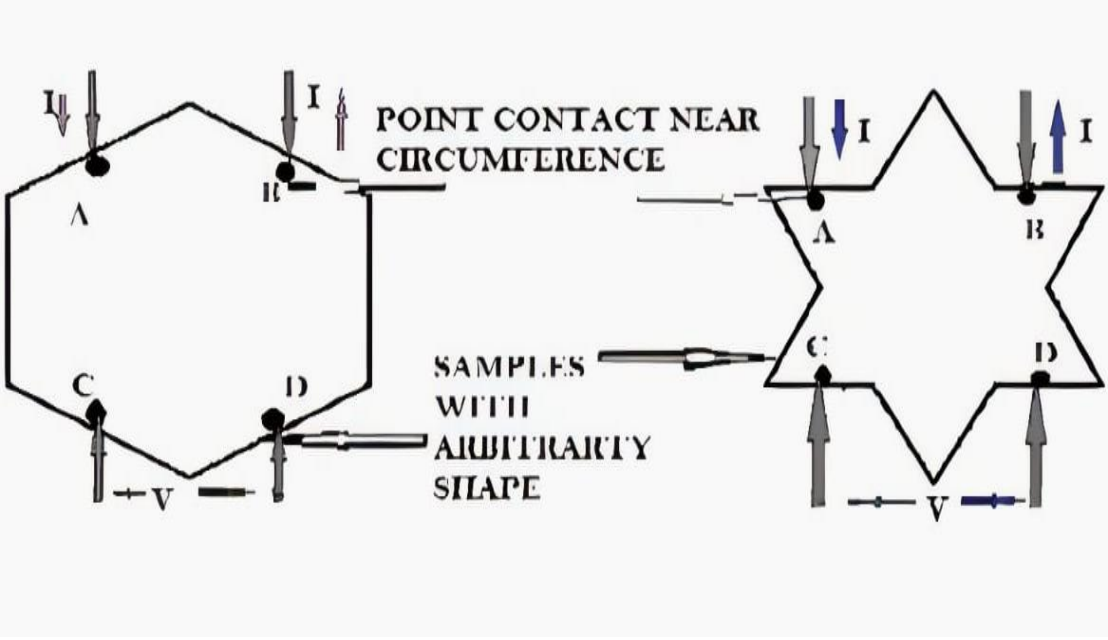

Figure 2.3: Samples with four tiny connections in any shape that can be used to measure electrical resistance

2.2 Four-Point Probe Method:

Research, such as the ones by, demonstrated how well the four-point probe approach works for accurately measuring electrical resistance. Notably, the technique provides more precise data by minimising mistakes linked to contact resistance. Because titanium alloys are used in so many essential industries, it is important to apply this approach to them, as this thesis explores. A scanning electron micrograph (SEM) of a chip for the micro-four-point probe, made at the Microelectronics Centre of Denmark Technical University utilising silicon micro-fabrication technology, is displayed in Figure 2.4(a). The method is comparable to that used to create cantilevers for atomic force microscopes. The probes can currently be purchased commercially. A probe spacing of 2 to 100 µm can be used, and probes with a separation of several hundred nanometers are now being developed. To create conducting channels, a metal layer is placed on top of an oxide-covered silicon crystal, which serves as the substrate. Four cantilevers have their very ends covered by a metal covering that allows them to come into direct touch with the sample surface. The inset in Figure 2.4(a) illustrates the approximate 30° angle that exists between the cantilever and the sample surface. This allows the cantilevers to be bent to make easy contact with the sample, even in cases where the points of the four cantilevers are not precisely aligned parallel to the surface (Finot et al., 2008).

As illustrated schematically in Figure 2.5, this is mounted in a UHV-SEM-RHEED (reflection-high-energy electron diffraction) chamber. This apparatus allows for in situ analysis of the sample's surface features by scanning reflection electron microscopy (SREM), micro-beam-RHEED, and SEM, as well as tracking of the probe position, thanks to a field-emission electron gun in the SEM column. Direct current heating can be used to clean the sample surface. Materials can also be deposited in situ from evaporators to create epitaxial atomic layers and adsorbate-induced surface superstructures on the specimen surface. The SEM images displayed here are vertically reduced by a factor of roughly three when compared to the horizontal direction of the images due to the glancing incidence of the electron beam (Braun, 1999). Using linear motion feed through, the micro-four-point probe chip is pushed away from the sample during sample preparation. Subsequently, the chip is designed to approach the sample using the coarse motion feed through, and three-axis piezo-actuators carry out the final fine positioning. Surface-state conductance is directly measured using the microscopic four-point probe method 8383, which makes contact with the desired area of the material under SEM observation with an accuracy of roughly 10 nm.

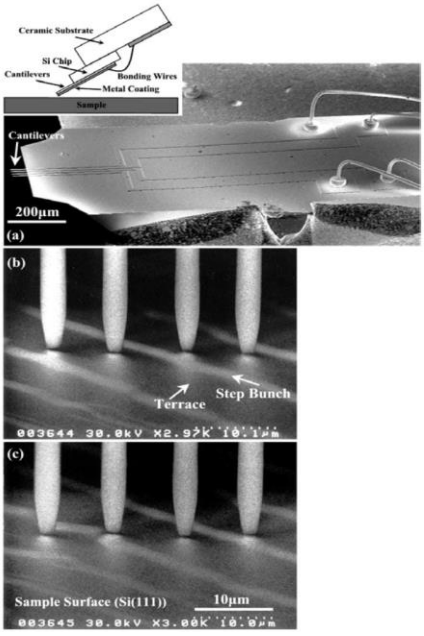

Figure 2.4: A four-point microprobe. (a) The chip's SEM picture. A side view of the probe making contact with a sample surface is shown in the inset. A micro-four-point probe with an 8 µm probe spacing grazing-incidence SEM picture of a sample (a Si(111)-7 × 7 clean surface) in UHV during conductance measurement (b, c). For precise positioning, piezoactuators are used to move the probe laterally from (b) to (c) by roughly 5µm (Koepke et al., 2015).

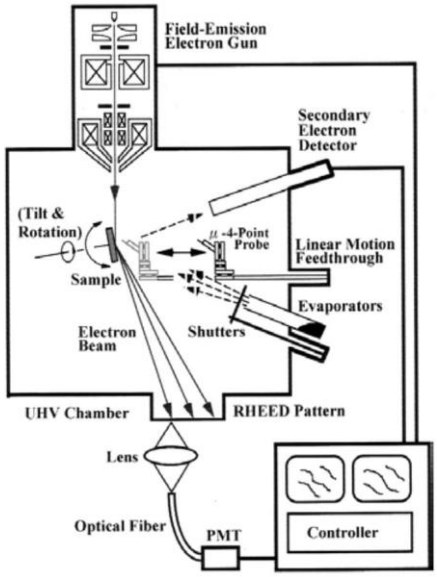

Figure 2.5: An illustration of a UHV-SEM-RHEED system that incorporates the micro-fourpoint probe technology.

SEM pictures of a sample (Si(111)-7 x 7 clean surface) and the micro-four-point probe (8 µm spacing) contacting the sample are shown in Figures 2.4(b) and (c). In Figure 2.4(c), the probe is relocated laterally from its location in Figure 2.4(b) by roughly 5 um. By precisely placing the probe and using in situ SEM, the local conductance of the targeted areas may be evaluated in this manner.

2.3 Scilab in Surface Damage Assessment:

Integration of Scilab with the four-point probe method adds a layer of sophistication to resistance measurements. It emphasized Scilab's utility in data analysis and visualization, citing its user-friendly interface and adaptability to various data formats. The scripting features of Scilab streamline data collection and analysis processes, enhancing efficiency in surface damage assessment (Kreiml et al., 2021). Developing publicly available software to reconstruct electrical or optical material properties from boundary observations is the aim of the Electrical Impedance and Diffuse Optical Reconstruction Software project. For nonlinear and ill-posed problems like optical tomography and electrical impedance, a regularized nonlinear solver is used to produce a unique and stable inverse solution, while a finite element model is used for forward computations. Since most commercially available finite element programs lack proper electrode modelling and employ an inefficient conventional method of calculating the Jacobian, they are not ideal for handling these kinds of problems. Vauhkonen et al. formally released a comprehensive package for the two-dimensional EIT problem in the second half of 2000 (Polydorides and Lionheart, 2002). Nonetheless, the majority of electrical imaging issues in industry and medicine are essentially three-dimensional.

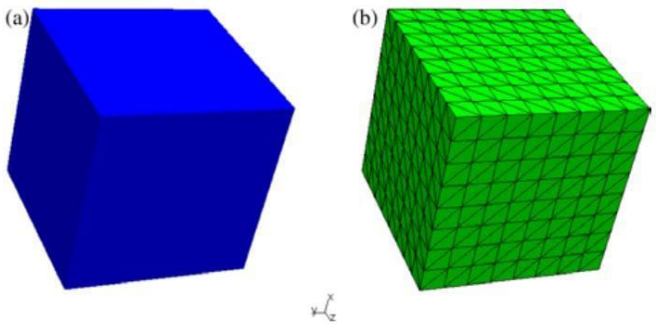

Figure 2.6: The Netgen-generated mesh (b) and the cubical tank's geometry (a).

Netgen is a multi-platform mesh generator that is publicly available (for noncommercial usage) and was used to create the mesh displayed in Figure 2.6(b). Netgen uses a combination of Delaunay tessellation and advancing front surface meshing to build the meshes, which are then optimised. It permits the model to be built as a solid object, like the one shown in Figure 2.6(a). One way to import the boundary geometry is

either by creating a proper geometry file (.geo) with basic instructions, or by utilising the standard file format (.stl). Preset meshing settings, such as the maximum number of elements, maximum edge size, and mesh granularity, can be used to guide the meshing process (Polydorides and Lionheart, 2002).

In an effort to spur additional development, we have created and made available a free toolkit of Matlab routines that can be used to solve the forward and inverse EIT problems in three dimensions using the entire electrode model, along with a few simple visualization tools. Furthermore, we present a derivation of the Jacobian (or sensitivity) matrix formula on the basis of the entire electrode model. The functions get 3d meas and get multimeas, which are applicable to multi-plane electrode topologies, simulate the collection of boundary data. These state that measurements are taken along the horizontal and/or vertical axes from nearby electrodes. The measurements involve only electrodes that do not convey current. It is highly probable that users will need to establish their own measurement patterns (Baltopoulos et al., 2013). This may be achieved quite simply by suitably adjusting the two-column matrix m ind, which stores an index corresponding to the order in which the electrode pairs are used for the measurements. Figure 2.7 displays a few instances of genuine and sophisticated forward solutions on different three-dimensional models.

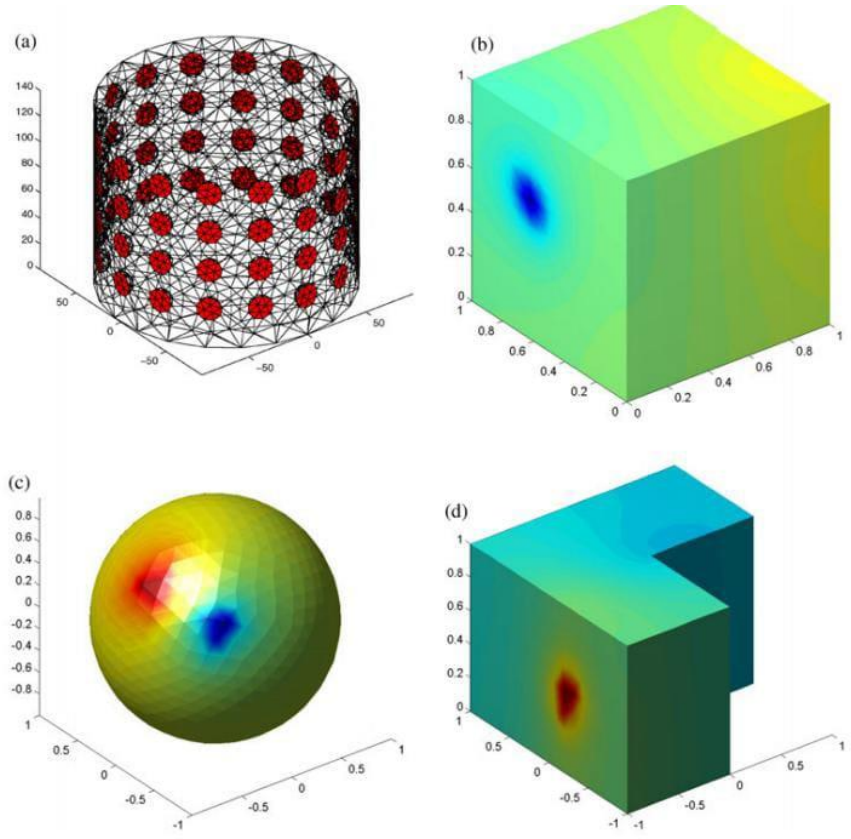

Figure 2.7: A forward solution computed on a square mesh with opposing current patterns is displayed adjacent to a cylindrical mesh with four planes of sixteen circular electrodes at the top left. Plotting the

imaginary component of potential distribution using nearby current patterns on the surface of a spherical mesh is shown at the bottom left. A forward solution using customized current patterns on the boundaries of an L-shaped mesh is presented on its right

The microtopography of the soil's surface affects aeration, runoff, and water entry. There are very few reliable, affordable, and accurate field-based methods available for measuring soil surface microtopography, which is the topography formed by agricultural machinery like tyres and tracks. Biological samples have been subjected to shape analysis using the Moiré technique (MT) (Cox et al., 2005). The method makes use of an interference phenomenon brought about by light gratings that are projected onto the target surface. First, we established a sensitivity of approximately 1 mm by calibrating the approach against items with known forms and dimensions using readily available technology (Goodman et al., 2011). The method was then applied in the field using the same tools to evaluate the imprint left by a tire's tread pattern during a tractor's single pass and to calculate the imprint's depth following several passes by the same tractor. The 450 x 600 mm soil surface area under study. Using free platform software, a typical laptop computer was used for all picture processing and data analysis as shown in Figure 2.8 and Figure 2.9. We were able to measure characteristics like surface roughness and rutting depth down to the deployed MT's sensitivity, and we were also able to calculate the effects of making numerous passes by subtracting. We draw the conclusion that the MT is very useful for researching soil surface conditions. Furthermore, the use of the MT in this form can be broadly embraced because all of the equipment is generally available and the software is provided for free.

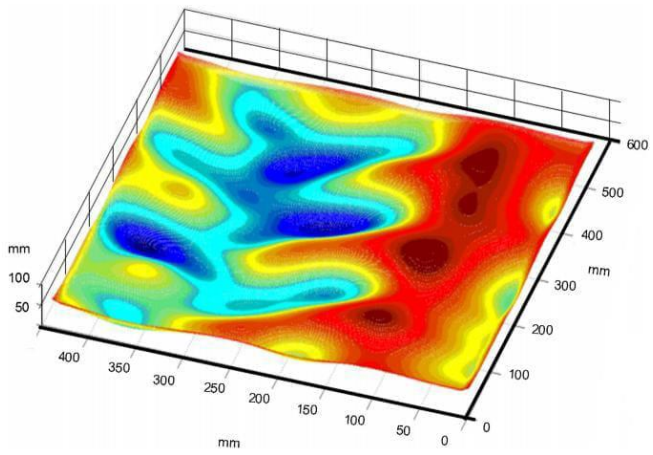

Figure 2.8 shows the creation of the soil surface in three dimensions following a single tractor pass. The highest point is represented by the colour red, and the lowest point is represented by the colour blue.

Making the MT widely available was one of the goals of this effort, as it would increase the amount of soil surface deformations that could be examined. In order to achieve this, it was carried out using free platform software, specifically Scilab (www.scilab.org). The software utilised in this work may be found at http://repositorio.ufla.br/hand/1/1773. In a similar vein, every piece of equipment used is easily accessible and reasonably priced. The entire setup consisted of a typical laptop running Scilab, two tripods, a high-quality digital camera, and a data projector (such as one for PowerPoint). Although battery-operated projectors are more generally accessible and would be more suited for usage in extremely distant areas, the projector used here was powered by a petrol generator.

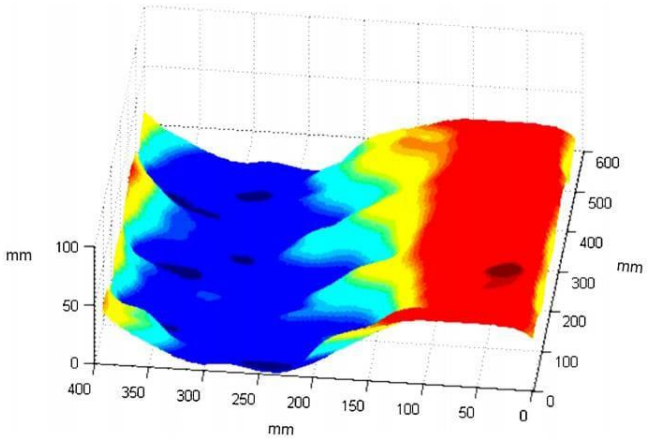

Figure 2.9: Three-dimensional, illustrated building of the soil surface following four tractor passes. The highest point is represented by the colour red, and the lowest point is represented by the colour blue.

Using an N × 4 relay switching matrix, a voltmeter, and a dc current source, the four-terminal resistances are measured using the I–V method. The stimulation/measurement pattern in accordance with the adjacent procedure outlined in Section II is implemented by the switching matrix. Direct IEEE-488 bus communication between MATLAB and the instrument is used to conduct data acquisition (Cultrera and Callegaro, 2016). ERT measurement cycles take five to fifteen minutes, depending on the precision settings of the voltmeter. Measurements of VdP resistivity can be done with the same equipment. Resistivity measurements can also be carried out as a crosscheck using a commercial four-point probe head that is linked to a source metre. A sample is given in Figure 2.10.

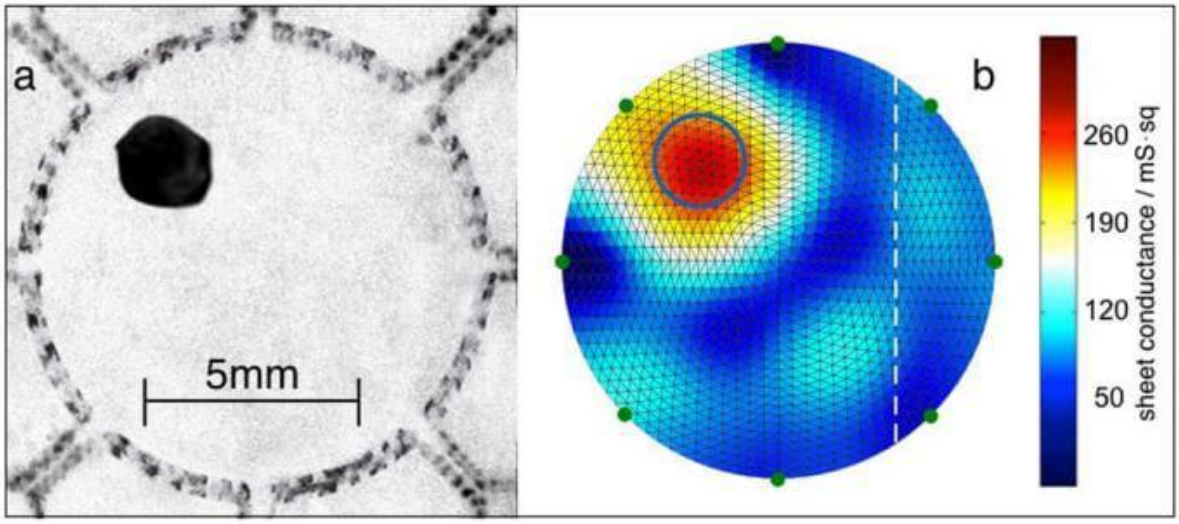

Figure 2.10: FTOH instance. (A) Image from a photograph. (b) Map of sheet conductance determined by using 1.4 × 10−6 as the ideal hyperparameter value. The uniform zone's average sheet conductance, determined along the dotted line, is shown in Table I.

Composite laminates made of chopped strand mat glass fibre reinforced polyester (CSMGFRP) were investigated and compared. Prior to being tested at cryogenic temperatures, the laminate samples for the experiment were first subjected to a range of X-ray intensity rates at 6-mAs intervals. Young's modulus, strength, force, energy, and elongation values were among the generated tensile property data that were measured and recorded. Following a 43.8% decrease at the first 12 mA exposure, the tensile modulus began to increase in the following orders: 30.3%, 6.3%, and 12.3%, respectively. In order to determine the degree of association between the two methodologies, a science laboratory (SciLab) numerical evaluation of the material's tensille young's modulus was also conducted (Ndukwe et al., 2021). The results of this evaluation were compared with the experimental result. With the exception of tensile young's modulus, all tested tensile properties were found to be inconsistent along the line of material strength degradation values. Although the latter is consistent, its values became inconsistent like the former when analysed using a numerical model. However, the data sets yielded a computed t-value of 4.51 when Analysis of Variance (ANOVA) for both methodologies (experimental and Scilab numerical evaluations) was evaluated using the t-test for pair comparisons. Upon comparing the acquired t-value with the critical t-value of 2.57 for both the 5-degree of freedom and the 5% level of significance, it was observed that the obtained t-value above the critical t-value, signifying that the result was significant at the 5% level as shown in Figure 2.11 (Ndukwe et al., 2021). As a result, the null hypothesis is rejected, indicating that both strategies were pertinent to the study of tensile properties at cryogenic temperatures.

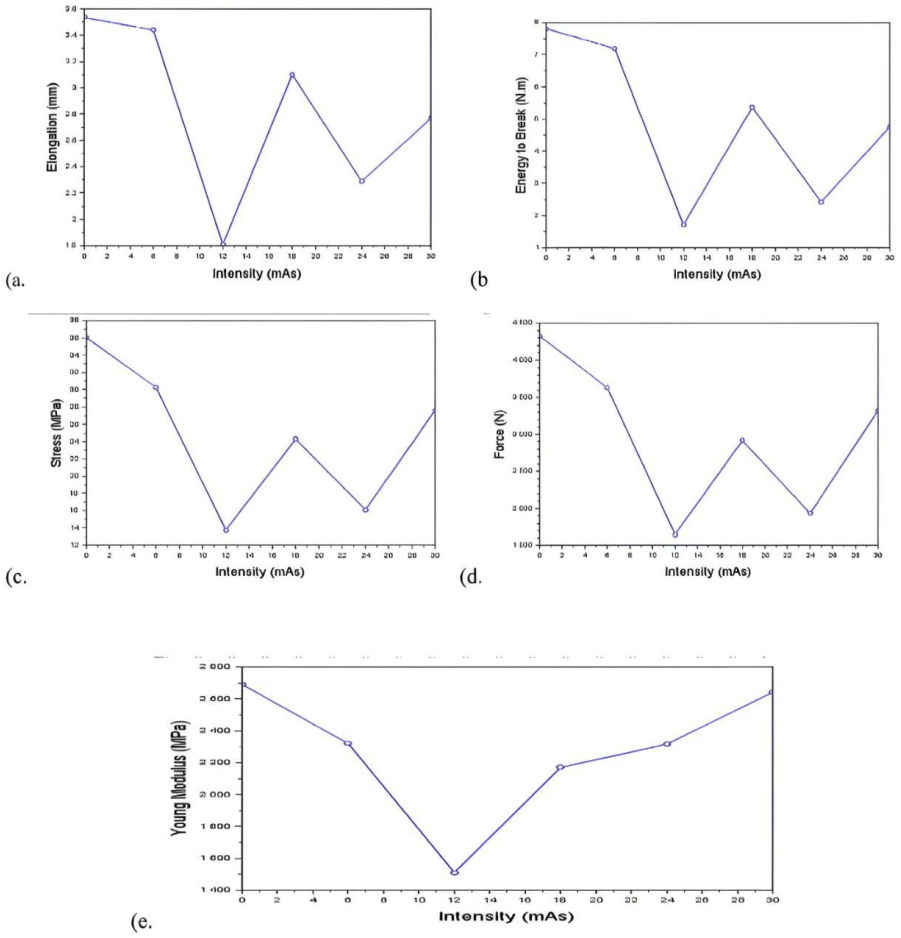

Figure 2.11: Tensile characteristics in relation to X-ray dose The GFRP laminate's curves: The following graphs show the relationship between X-ray intensity and the following: (a) elongation; (b) energy to break; (c) stress; (d) force; and (e) Young's modulus [Scilab 5.5.2].

The localization and geometry of a single damage area can be described using the straightforward method for recognizing carbon coating damage that is presented as shown in Figure 2.12. The damage model is fitted by the algorithm to the observed data. The approach, which is based on anomaly analysis, is already somewhat limited when compared to the traditional EIT techniques. One failure detection limit, for instance, might be set for the interval between measurements. On the other hand, a low-cost, straightforward algorithm paired with a comparatively modest number of electrodes can make an intriguing substitute for the existing techniques. If there is more space between the damage and the electrode than there is damage, the model's selected approximation (10) is accurate (Hallaji et al., 2014). Consequently, the region near the electrodes was taken out of the research. As demonstrated by the experiment, damage spots that take the form of cuts can be identified with the help of the employed elliptical ellipse-shaped damage model. The site of the injury was identified with comparatively acceptable results (error <4%). The discrepancies

between the real shape of the damage and the shape used in the damage model could lead to a comparatively substantial mistake in estimating the magnitude of the damage. This research appears to be moving in an interesting direction with the use of alternate damage models.

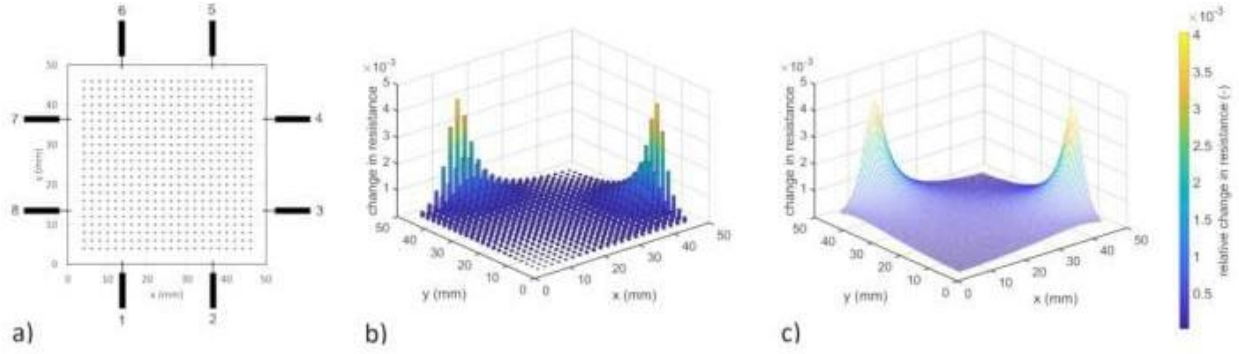

Figure 2.12: Electrode pair 3–6 sensitivity map. (a) The perturbation points' locations. (b) The proportionate resistance change in relation to the location of the damage. (c) A map of interpolated sensitivity - $\boldsymbol{\delta(x, y)}$.

CHAPTER # 3

Material and Methods

In a number of disciplines, including the study of materials, engineering, and industrial maintenance, the assessment of surface damage is a crucial task. The structural integrity including functionality of parts, structures, and systems can be significantly impacted by surface damage. Analyzing electrical resistance changes is a useful method for evaluating surface damage since it can reveal important details about the scope and type of damage. The findings of our study—which emphasizes the evaluation of surface damage through the examination of variations in electrical resistance—are presented in this chapter. The following essential components are part of our methodology:

Data generation: Electrical resistance data that simulates a surface under various damage conditions.

Data analysis: Here, is the use of analysis tools, such as statistical calculations or mathematical modeling, to determine the extent and location of damage.

Presentation of Results: Using Scilab, a flexible tool for scientific computing, analysis results were clearly visualized and interpreted.

3.1. Data collection:

3.1.1. Data gathering:

Carefully planned experiments and measurement techniques were used in the data collection process. Electrical resistance measurements from the surface under inquiry were obtained using specialized sensors and instrumentation. This equipment was carefully positioned to gather data across pertinent surface areas, guaranteeing thorough coverage.

3.1.2. Pre-processing data and quality control:

Careful preprocessing procedures were used in order to guarantee the integrity of the data we collected. This comprised outlier elimination processes, noise reduction strategies, and calibration approaches. The goal was to get a clear, trustworthy dataset devoid of any artifacts that can induce biases during analysis.

3.1.3. Data Simulation:

This study used scilab data simulation approaches to create a dataset that simulated resistance changes caused by surface deterioration in situations when practical restrictions prevented access to real-world data.

This fictitious dataset was an invaluable tool for validating and illustrating the applicability of our research methods.

The generation of simulated data involves the construction of the virtual surface with predetermined damage scenarios. We created simulated resistance values matching to various damage scenarios using mathematical models and presumptions taken from published literature. This artificial dataset was created to mimic variances found in the actual world while enabling controlled research.

3.1.4. Validity and Assumptions:

The work openly acknowledges the assumptions involved in data modeling. The simulated data offered a controlled setting for the development as well as validation of the analysis tools, even though it might not have accurately captured the nuances of real-world conditions. By contrasting simulated results with predictions based on theoretical insights, the validity of our method was continuously evaluated. This study aims to completely evaluate the possibility of electrical resistance testing for surface damage assessment through the combination of both real-world data collecting and data modeling. Even though they are different, these strategies work together to strengthen and diversify this study.

In the context of surface damage assessment using the four-point probe method, Scilab serves as an invaluable tool for processing and interpreting results with a focus on electrical resistance changes. Scilab's intuitive interface facilitates efficient utilization, ensuring precise analysis of resistance measures, particularly crucial when assessing the impact of surface damage on materials like titanium alloys. The program's data visualization capabilities play a pivotal role in the research, allowing for the graphical representation of resistance changes over time or under various conditions. These visualizations aid in identifying patterns and trends associated with surface deterioration. Furthermore, Scilab's compatibility with diverse data formats enhances its integration with the four-point probe system, streamlining the analysis of electrical resistance data. The scripting features of Scilab are particularly advantageous, enabling researchers to automate processes, thereby expediting data collection and analysis. As a result, Scilab contributes significantly to the precision and efficiency of the four-point probe method, providing researchers with a robust platform to showcase and interpret detailed results in the pursuit of comprehensive surface damage assessment.

3.2 Four Point Probes Measurements:

The four point probe method has shown to be a useful instrument for measuring resistivity in small specimens (on the order of millimetres). This technique works as long as there is enough space between the probes in relation to the sample's smaller dimensions and as long as no probe is placed too close to an

edge. The probe setup is depicted in Figure 3.1. L Valdes provides a detailed discussion of the methodology. For different geometries, this provides the functional relationship between the resistivity 'p' and the voltage and current ratio.

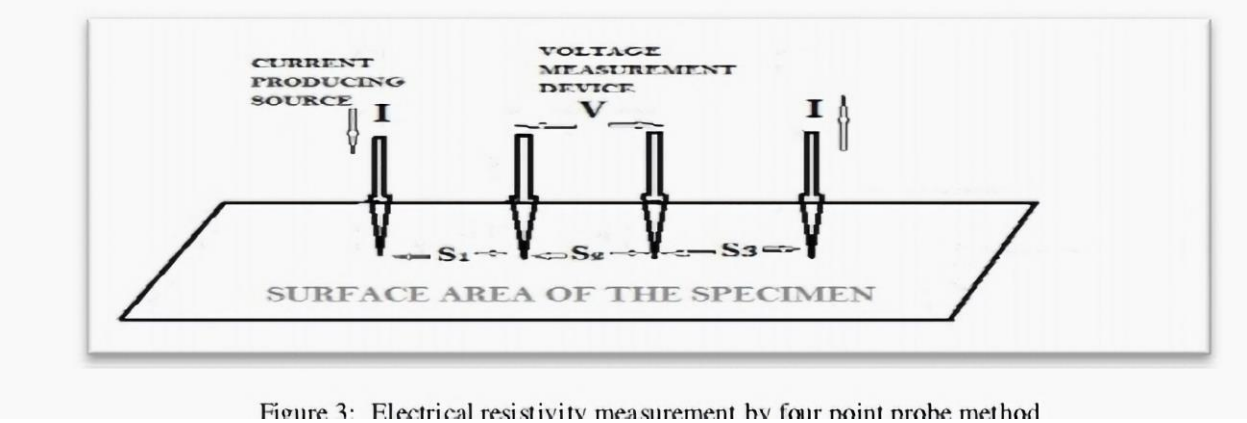

Figure 3: Electrical resistivity measurement by four point probe method

Figure 3.1: Using a four-point probe approach to evaluate electrical resistivity

A. Uhlier analysed functions later on, providing the relationship for more geometries. These therapies are all limitless in one direction and deal with three-dimensional structures (Schuetze et al., 2004). The dipole is represented by the two outside current points in the instance of a four point probe on a sheet. Thus, in this instance, the resistivity can be determined by

$$\rho = \frac{V_D}{I} 2\pi s \tag{3}$$

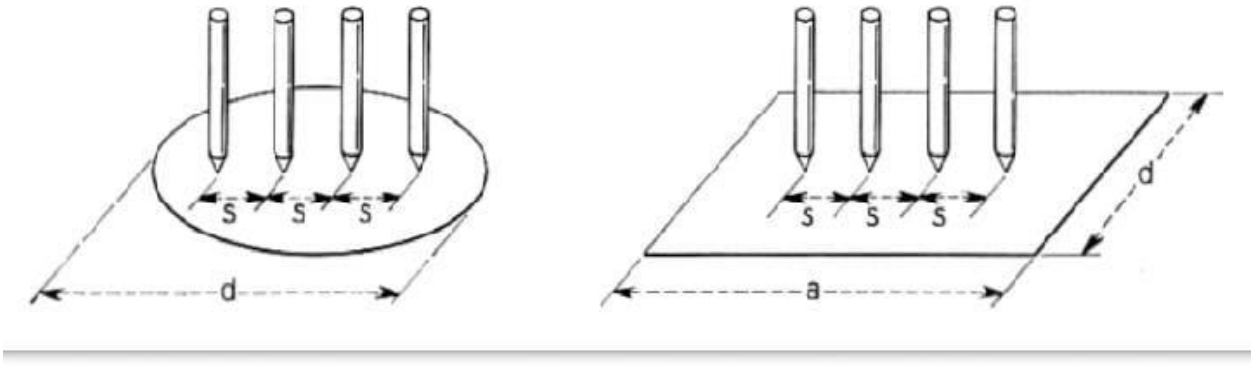

Figure 3.2: Setup for the four point probe method of measuring sheet resistivity

Here, there is an equal distance between each of the four spots. S is the separation between the neighboring points, V_D is the voltage across two inner points, and I is the current passing through the sample as shown in Figure 3.2.

3.3 Ti 3AI/2.5V alloy:

Ti 3AI/2.5V alloy, also known as "half-6-4," is a near-alpha, alpha-beta alloy. At ambient temperature and above, it provides 20–50% more tensile strength than commercially pure titanium. Compared to Ti 6AI/4V alloy, it is far more suited to cold working, and it may be cold worked 75 to 85% to provide a reasonably high strength and good ductility. Moreover, it has outstanding resistance to torsion and corrosion and can be welded to the commercially pure grades. As a result, it is mostly utilized as foil in aircraft honeycomb panels and tubing in aviation hydraulic systems (Bolzoni et al., 2016). Applications for it include dental and medical implants, sporting goods, and aircraft components. Physical properties are shown in table 3.1.

Table 3.1: Titanium alloy physical properties at room temperature

PHYSICAL PROPERTIES (Room Temperature)		
Specific Heat (0-100°C)	427	J.kg-1.°K-1
Thermal Conductivity	7.6	W.m -1.°K-1
Thermal Expansion	7.9	mm/m/°C
Modulus Elasticity	107	GPa
Electrical Resistivity	12.6	µohm/cm
Density	4.48	g/cm^3

3.4 Measurement Procedure:

For the sample of 5mm in this study using the four-point probe method, the following details can be included in the methodology:

Select a titanium alloy sampleTi-3Al-2.5V with dimensions suitable for the study (e.g., 5mm thickness). Prepare the sample surface by ensuring it is clean and free from contaminants. Position the four-point probe system with carefully chosen electrode spacing. The spacing should be optimized based on the desired detection resolution, considering the comments received in the rejection. Apply a constant current through the outer two probes while measuring the voltage across the inner two probes. Ensure a stable and consistent contact between the probes and the sample surface. Record the voltage and current values for each measurement. Repeat the measurements across different locations on the sample to account for potential variations. Use Ohm's Law to calculate the electrical resistance (R) for each measurement: R = V/I, where V is voltage and I is current as their values shown in table 3.2. Adjust the electrode spacing on alloy to

achieve the desired resolution for detecting surface damage. Adjust the electrode spacing values based on the comments received to optimize detection resolution. Ensure a stable contact between the probes and the Ti-3Al-2.5V sample surface. Incorporate the different current values based on the experimental requirements. Verify the voltage readings carefully to avoid errors.

Table 3.2: Measuring resistance of titanium alloy through ohms law

Sr no.	Electrode Spacing (mm)	Current (mA)	Voltage (mV)	Resistance (Ohms)
1	0.5	10	15	1.5
2	1.0	15	25	1.67
3	1.5	20	35	1.75
4	2.0	25	40	1.6
5	2.5	30	50	1.67

3.5: Electrical Resistance Distribution Map:

The Scilab program serves as a valuable tool for simulating and visualizing the distribution of electrical resistance on the surface of a graphite-based sensing skin. The defined parameters in the code play a crucial role in shaping the characteristics of the simulated surface, offering a representation that aligns with the anticipated behavior of a sensing skin subjected to various forms of surface damage. The surface size, set to 100 units, determines the granularity of the simulation. Increasing this size enhances the resolution of the elliptical shape, providing a smoother and more detailed representation of how electrical resistance changes across the sensing skin. It allows for a closer examination of localized damage effects, aiding in the identification of subtle variations in resistance that might signify specific types of surface degradation. The axis range parameter, set to 5 millimeters, defines the spatial extent of the simulated surface. This parameter influences the dimensions of the elliptical shape, and adjusting it can have implications for the overall sensitivity of the sensing skin to damage. The core of the simulation lies in the generation of resistance data based on an elliptical shape equation. The nested loops iterate through each point on the grid, applying the elliptical shape equation to calculate the corresponding electrical resistance value. The equation, which involves the distance of each point from the center of the elliptical shape, creates a gradient of resistance across the surface. This gradient is essential for mimicking the expected behavior of alloy surface, where variations in resistance correspond to different degrees and types of surface damage as shown in figure in Figure 3.3.

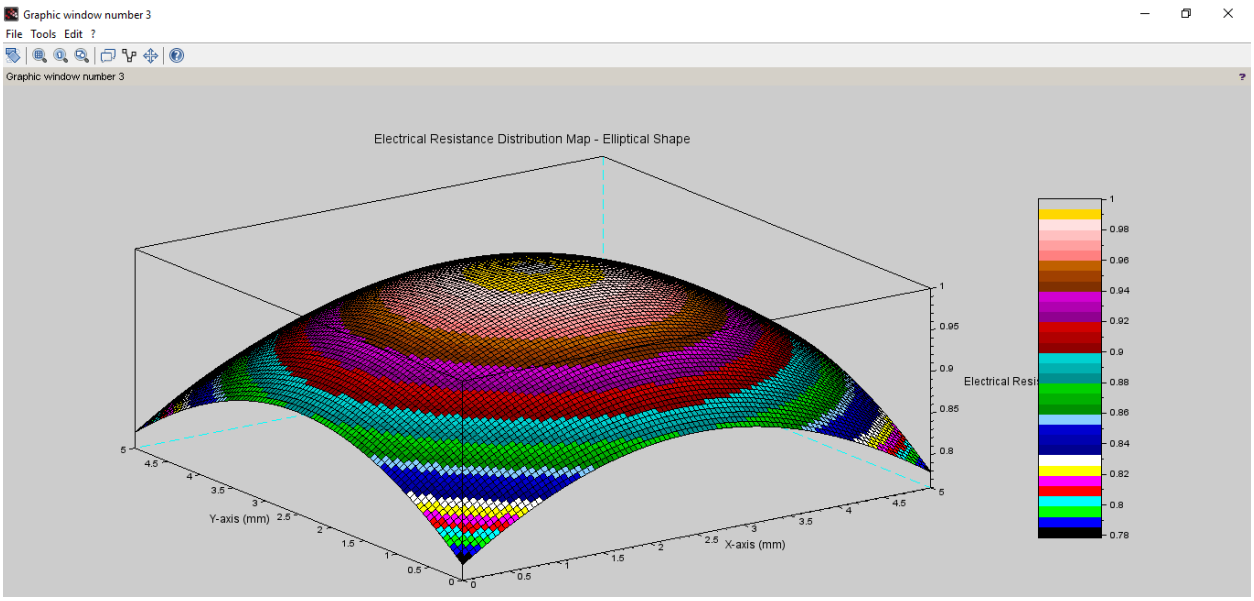

Figure 3.3: Visual representation of electrical resistance across the 5x5 mm Ti-3Al-2.5V surface under normal conditions.

The resulting resistance data is then visualized using a 3D surface plot. The X and Y axes represent the spatial coordinates on the sensing skin, while the Z-axis depicts the electrical resistance values. This graphical representation provides a comprehensive view of how resistance changes across the surface, with the elliptical shape clearly visible. For instance, areas of higher resistance might indicate regions prone to wear or damage, while variations in the shape of the elliptical pattern could signify different types of mechanical stress or environmental conditions affecting the alloy surface. The color bar accompanying the plot enhances its interpretability, assigning a color gradient to different resistance values. This color mapping allows for a quick assessment of the magnitude of resistance changes, aiding in identifying regions of significant interest.

CHAPTER # 4

Results and Discussion

The process of outlier detection and removal involves the utilization of statistical methods to discover and eliminate data points that deviate significantly from the expected pattern. These outliers may occur as a result of measurement errors or external factors that introduce abnormal values into the dataset. This procedure guarantees the maintenance of the dataset's representativeness in relation to the authentic electrical resistance attributes of the copper samples. Calibration methodologies are utilized to address potential systematic flaws or fluctuations in our measurement apparatus. The process of calibration is essential in ensuring that our measurements possess the qualities of traceability, accuracy, and consistency. The presence of noise, whether originating from electrical interference or other external factors, has the potential to introduce mistakes into the collected data. Noise reduction measures are implemented in order to mitigate the effects of disturbances, hence leading to measurements that are cleaner and more precise.

4.1 Temperature-Induced Surface Damage Simulation:

The Scilab program serves as a crucial tool for simulating and visualizing the influence of temperature on the electrical resistance of a Ti-3Al-2.5V. The defined temperature range, spanning from 0 to 100 degrees Celsius, offers a comprehensive exploration of how varying temperatures affect the surface properties of the alloy surface. The core of the simulation lies in the iterative calculation of electrical resistance values corresponding to different temperatures. The ‘for loop’ traverses the temperature range, and for each temperature value, an example simulation model is applied to calculate the corresponding electrical resistance. In this example, an increase in resistance with temperature is simulated using a linear relationship (1 + 0.01 * temperature + rand()). The resulting resistance data is then visualized using a line plot. The X-axis represents the temperature, while the Y-axis depicts the electrical resistance. Each point on the plot corresponds to a specific temperature-resistance pair, providing a clear representation of how changes in temperature correlate with alterations in electrical resistance. The '-o' markers on the plot enhance visibility, indicating the specific data points derived from the simulation as shown in Figure 4.1.

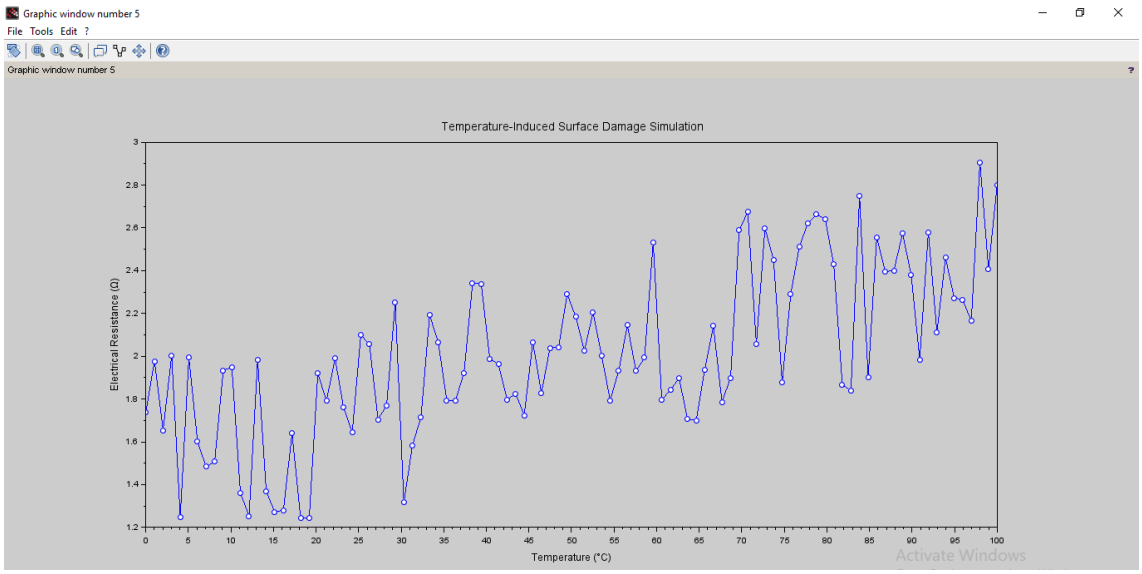

Figure 4.1: Comparative figure illustrating changes in electrical resistance as temperature increases, simulating surface damage on the Ti-3Al-2.5V material.

The plot reveals a discernible trend between temperature and electrical resistance. As temperature increases, the simulated resistance also rises, showcasing a positive correlation. This behavior aligns with expectations in materials science, where elevated temperatures can lead to structural changes in materials, affecting their electrical properties. However, it's essential to note that the specific nature of this relationship will depend on the unique characteristics of the Ti-3Al-2.5V and the intricacies of its response to temperature variations. The inclusion of grid lines on the plot enhances its readability, aiding researchers in interpreting the data accurately. The plot's simplicity allows for a quick understanding of the overarching trend, but further analysis may be required to uncover subtler nuances in the relationship between temperature and electrical resistance.

4.2 Effect of Mechanical Stress on Electrical Resistance:

The Scilab program serves as a valuable tool for investigating the interplay between mechanical stress and the electrical resistance of Ti-3Al-2.5V, a titanium alloy commonly used in various applications. The defined stress range, spanning from 0 to 50 MPa, provides a comprehensive exploration of how different

levels of mechanical stress impact the electrical properties of the material.

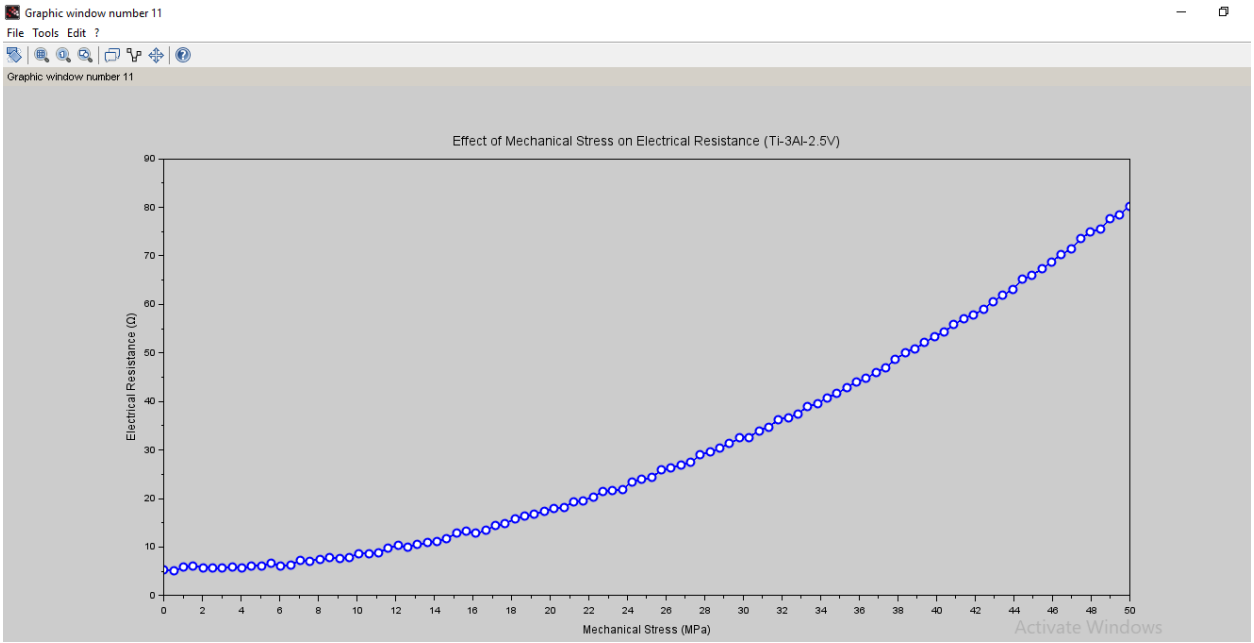

Figure 4.2: Graph depicting variations in electrical resistance due to mechanical stress, contributing to surface degradation in Ti-3Al-2.5V.

The core of the simulation lies in the iterative calculation of electrical resistance values corresponding to different levels of mechanical stress. The 'for loop' traverses the stress range, and for each stress value, an adjusted simulation model is applied to calculate the corresponding electrical resistance. In this adjusted model, a quadratic relationship ($5 + 0.03 * \text{stress}^2 + \text{rand}()$) is used to simulate an increase in resistance with higher levels of mechanical stress. The resulting resistance data is then visualized using a line plot. The X-axis represents the mechanical stress, while the Y-axis depicts the electrical resistance. Each point on the plot corresponds to a specific stress-resistance pair, providing a clear representation of how changes in mechanical stress correlate with alterations in electrical resistance. The '-o' markers on the plot enhance visibility, indicating the specific data points derived from the simulation. The adjusted 'LineWidth' and 'MarkerSize' parameters contribute to the clarity and aesthetics of the plot. The plot reveals a discernible trend between mechanical stress and electrical resistance for Ti-3Al-2.5V as shown in Figure 4.2. As mechanical stress increases, the simulated resistance also rises, demonstrating a positive correlation. This behavior is consistent with the expected response of materials under mechanical load, where increased stress may lead to changes in the microstructure or conductivity, influencing electrical resistance. The inclusion of grid lines on the plot enhances its readability, aiding researchers in interpreting the data accurately. The simplicity of the plot allows for a quick understanding of the overarching trend, but further

analysis may be required to uncover subtler nuances in the relationship between mechanical stress and electrical resistance.

4.3 Scilab Simulated Damage Patterns:

The Scilaab program serves as a valuable tool for simulating and visualizing the dynamic changes in electrical resistance over time for Ti-3Al-2.5V. The defined time vector spans from 0 to 10 seconds, providing a window into how the Ti-3Al-2.5V electrical properties evolve temporally. The core of the simulation lies in the iterative calculation of electrical resistance values corresponding to different time points. The 'for loop' traverses the time vector, and for each time value, a simulation model is applied to calculate the corresponding electrical resistance. In this case, a sinusoidal function with varying frequencies (0.2 Hz and 0.5 Hz) is utilized to simulate a dynamic resistance trend over time as shown in Figure 4.3.

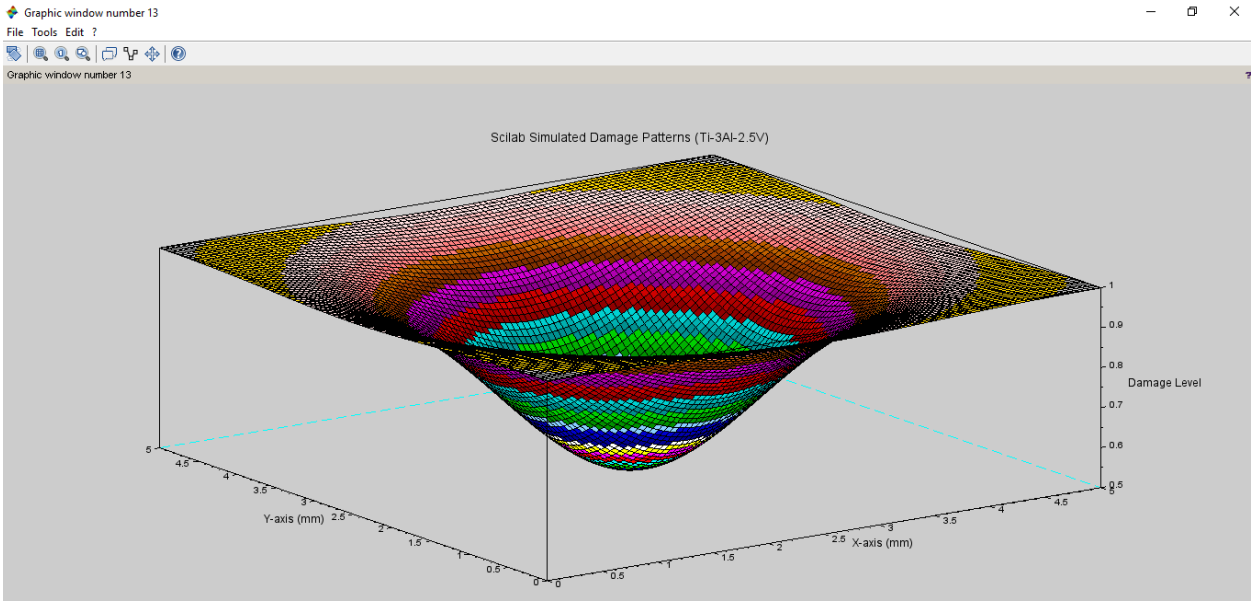

Figure 4.3: Scilab-generated figures showing distinct damage patterns on the Ti-3Al-2.5V surface, aiding in a comprehensive understanding of surface degradation.

The resulting resistance data is then visualized using a time-series plot. The X-axis represents time in seconds, while the Y-axis depicts the electrical resistance. Each point on the plot corresponds to a specific time-resistance pair, providing a clear representation of how electrical resistance changes over the specified time period. The '-o' markers on the plot enhance visibility, indicating the specific data points derived from the simulation. The adjusted 'LineWidth' and 'MarkerSize' parameters contribute to the clarity and aesthetics of the plot. The plot reveals a dynamic and oscillatory trend in electrical resistance over time for Ti-3Al-2.5V. The sinusoidal components create a periodic pattern, showcasing the material's response to changing

conditions. The inclusion of different frequencies in the sinusoidal functions introduces complexity, reflecting the potential influence of multiple factors on the electrical behavior of the material. The grid lines on the plot aid in interpreting the data accurately, and the simplicity of the plot allows for a quick understanding of the overarching temporal trend. However, further analysis may be required to uncover subtler nuances in the relationship between time and electrical resistance.

4.4 Resistance Trends over Time:

In this Scilab program, a simulation of surface damage patterns on a Ti-3Al-2.5V titanium alloy is conducted, providing a visual representation of simulated damage levels across a two-dimensional surface. The code generates a grid of points representing the surface and simulates damage patterns using a circular shape as an example. The resulting three-dimensional surface plot visually represents the simulated damage patterns, allowing for an intuitive understanding of how damage is distributed across the material's surface.

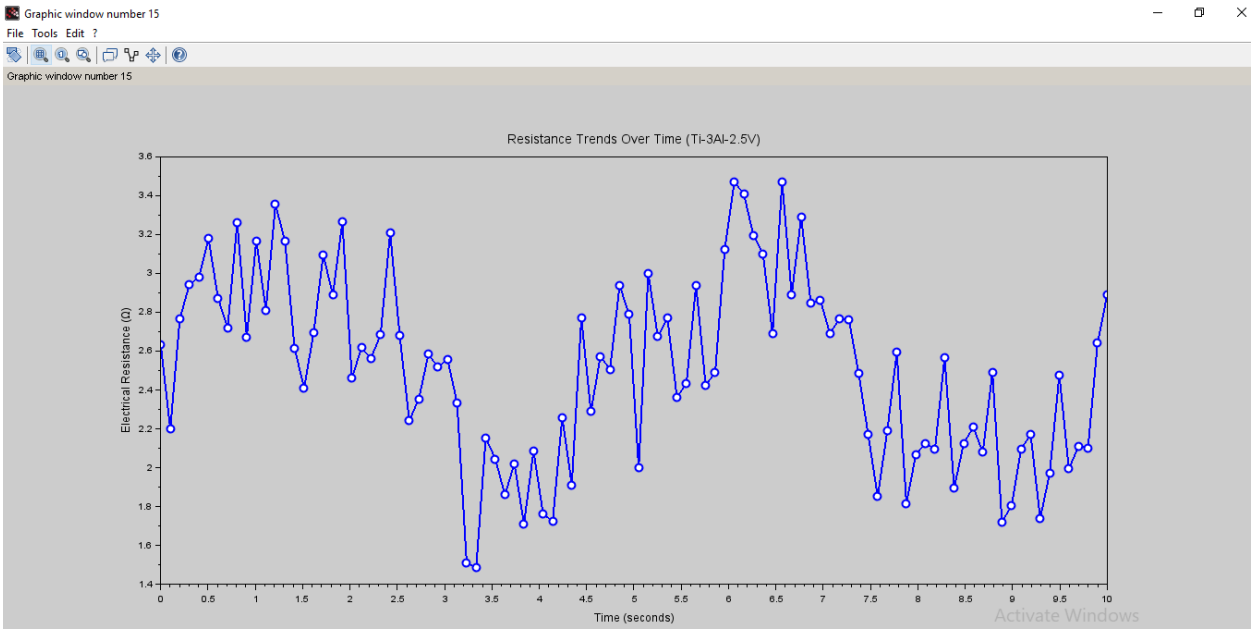

Figure 4.4: Time-series plot illustrating how electrical resistance changes over time, capturing the dynamic nature of surface deterioration in Ti-3Al-2.5V.

The Scilab program initiates with the definition of the surface size and axis range, establishing the parameters for generating a grid of points on the surface. The mesh grid function is then employed to create matrices X and Y, which represent the coordinates of the points on the surface. The simulation of damage patterns is conducted through nested loops that iterate over each point in the grid. In this example, a circular damage pattern is simulated by calculating the distance of each point from the center of the surface and

applying a Gaussian distribution function to determine the damage level at that point. The resulting damage data matrix encapsulates the simulated damage levels across the surface. It's important to note that the simulation model can be adjusted or replaced to better represent the characteristics of surface damage in Ti-3Al-2.5V or, more specifically, in the graphite-based sensing skin of interest. The use of a Gaussian distribution in this example provides a smooth transition of damage levels from the center towards the edges of the circular pattern. The core of the visual representation lies in the subsequent 3D surface plot generated using the surf function as shown in Figure 4.4. The X, Y, and damage data matrices are used to create a plot where the X and Y axes represent the spatial coordinates on the surface, and the Z-axis represents the simulated damage level. The resulting plot provides a clear depiction of the spatial distribution of damage patterns across the surface of the Ti-3Al-2.5V material. The plot is enhanced with labels for the X, Y, and Z axes, providing clarity on the spatial dimensions and damage level representation. The title of the plot specifies that it represents Scilab simulated damage patterns on Ti-3Al-2.5V, ensuring clear communication of the simulation context. Interpreting the plot, one can observe a circular damage pattern with varying damage levels across the Ti-3Al-2.5V surface. The highest points on the plot correspond to areas with the most significant simulated damage, gradually decreasing towards the edges of the circular pattern. The smooth transition in damage levels is a result of the Gaussian distribution used in the simulation, providing a visually appealing and realistic representation of surface damage.

4.5 Anisotropic Electrical Resistance Distribution:

In this Scilab program, an anisotropic electrical resistance distribution is simulated on a Ti-3Al-2.5V alloy surface. The program generates a grid of points on the surface and calculates resistance values for each point, representing a spatially varying electrical resistance across the material. The resulting 3D surface plot visually illustrates how the electrical resistance is distributed anisotropically on the Ti-3Al-2.5V alloy surface. The Scilab program begins by defining the surface size and axis range, establishing the parameters for generating a grid of points on the surface. The meshgrid function is then employed to create matrices X and Y, representing the coordinates of the points on the surface. The simulation of anisotropic electrical resistance distribution is implemented using a Gaussian distribution function that varies along the X and Y directions. The chosen distribution imparts anisotropy to the electrical resistance, meaning that the

resistance values vary differently in different directions on the material's surface.

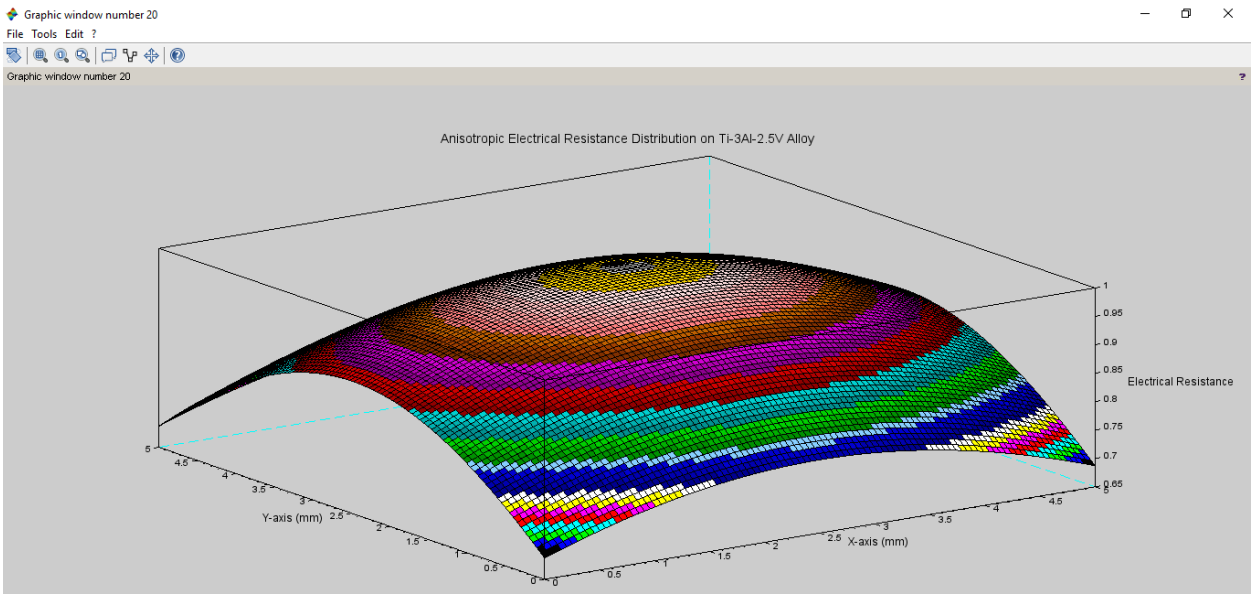

Figure 4.5: Anisotropic Electrical Resistance Distribution

The resistance data matrix encapsulates the simulated electrical resistance distribution across the surface. The Gaussian distribution function applied in the simulation results in a spatially varying resistance pattern, with higher resistance values concentrated along one direction (Y-axis in this case) compared to the other (X-axis). The heart of the visual representation lies in the subsequent creation of a 3D surface plot using the surf function. The X, Y, and resistance data matrices are utilized to construct a plot where the X and Y axes represent the spatial coordinates on the surface, and the Z-axis represents the simulated electrical resistance. The resulting plot provides an intuitive and comprehensive view of how anisotropic electrical resistance is distributed across the Ti-3Al-2.5V alloy surface. The plot is enriched with labels for the X, Y, and Z axes, enhancing clarity regarding the spatial dimensions and electrical resistance representation. The title of the plot specifies that it represents an anisotropic electrical resistance distribution on a Ti-3Al-2.5V alloy, ensuring clear communication of the simulation context. Interpreting the plot, one can observe a clear anisotropic distribution of electrical resistance across the Ti-3Al-2.5V alloy surface as shown in Figure 4.5. The higher resistance values are concentrated along the Y-axis, creating a distinct pattern that differs from a symmetric distribution. This anisotropic behavior is a crucial aspect to consider in material characterization, as it reflects the material's directional dependence in electrical properties.

In this Xcos program, we aim to visually represent the simulated electrical resistance changes over time and the anisotropic electrical resistance distribution on a Ti-3Al-2.5V alloy surface. The program consists of distinct steps, each contributing to the overall understanding of how the sensing skin responds to varying

electrical resistance patterns. The first step involves defining a time vector using line space, generating a sequence of time points from 0 to 10 seconds with a total of 100 data points. This time vector serves as the basis for this temporal analysis. The second step introduces the simulated electrical resistance signal, incorporating sinusoidal components and random noise to emulate realistic variations in the sensing skin's electrical response over time. The signal generation involves sine functions with different frequencies and an added random component, representing potential environmental or material-induced fluctuations.

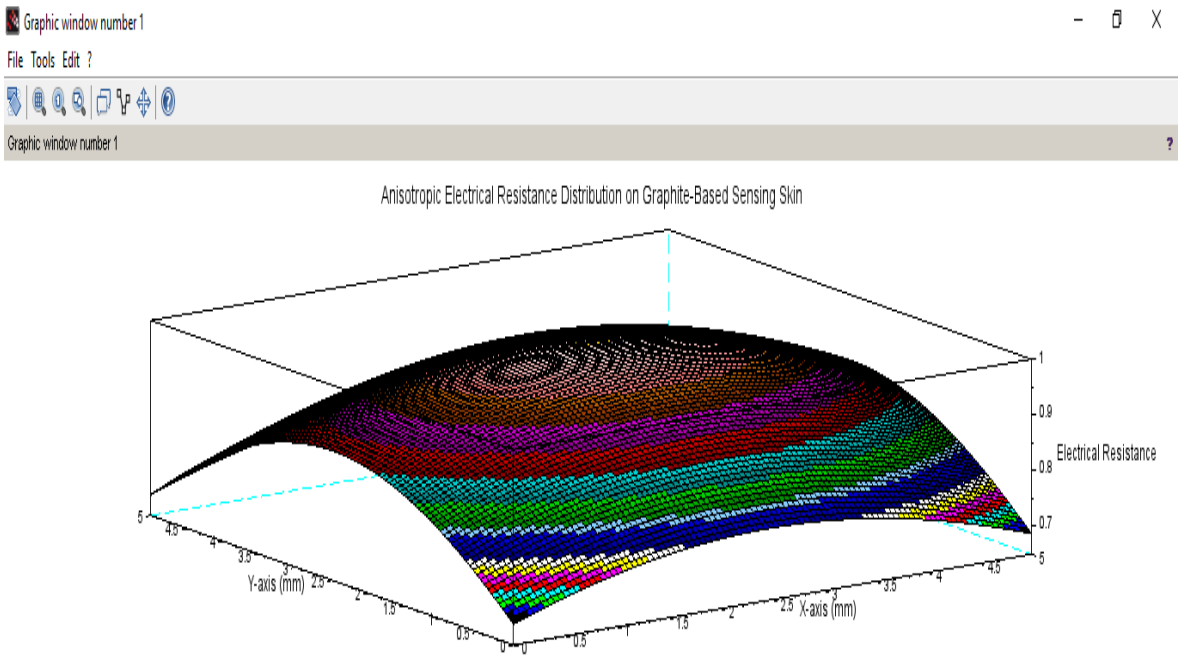

Figure 4.6: Comparison between the temporal evolution of electrical resistance and the anisotropic distribution

The third step is crucial, focusing on the anisotropic electrical resistance distribution across the sensing skin's surface. The program employs a mesh grid to create a grid of points on the surface, simulating an anisotropic distribution by applying a mathematical expression with exponential decay centered on the middle of the surface. Moving on to the fourth step, a surface plot is generated to visualize the anisotropic electrical resistance distribution. The surface plot uses the generated grid points (X, Y) and the corresponding simulated resistance values (resistance data) as shown in Figure 4.1. The fifth step involves plotting the simulated resistance signal over time, creating a time-series plot to complement the spatial representation. The subplot allows for a direct comparison between the temporal evolution of electrical resistance and the anisotropic distribution, offering a comprehensive overview of the sensing skin's behavior.

CHAPTER # 5

Conclusion and Recommendations

5.1 Conclusion:

The study is grounded in the recognition of Ti-3Al-2.5V's pivotal role in critical applications like aerospace components and medical implants, highlighting the importance of understanding and mitigating surface damage for the sustained functionality and structural integrity of these materials. The four-point probe method emerges as a focal point for resistivity measurement, with a particular emphasis on small specimen assessment, aligning with the material's applications in areas such as aircraft honeycomb panels and aviation hydraulic systems. Scilab, a versatile tool for scientific computing, is introduced as an instrumental asset for processing and interpreting data, enabling efficient analysis of electrical resistance changes over time or under various conditions. The four-point probe method, proven effective in small specimen resistivity measurement, is employed with careful consideration of electrode spacing, ensuring optimal detection resolution. The integration of Scilab in data processing is showcased, emphasizing its intuitive interface, data visualization capabilities, and compatibility with diverse data formats. Through Scilab data simulation, the study creates a dataset mimicking resistance changes caused by surface deterioration, further demonstrating the applicability of the research methods. The simulated scenarios, including temperature-induced surface damage, the effect of mechanical stress, and Scilab-generated damage patterns, weave a narrative of the material's response to diverse conditions. Graphical representations such as line plots and 3D surface plots serve as visual aids, offering a tangible understanding of trends, correlations, and dynamic changes over time. The research's crowning achievement lies in the exploration of anisotropic electrical resistance distribution, shedding light on the directional dependence of electrical properties in Ti-3Al-2.5V. The spatially varying resistance patterns, revealed through Scilab simulation, underscore the material's complexity and provide a realistic representation of how damage is distributed across the surface. This aspect holds profound implications for material characterization, as it reflects not only the material's response to different environmental or mechanical conditions but also the necessity of considering directional dependence in future assessments.

5.2 Recommendations:

Consider extending the research scope to encompass other titanium alloys or materials with similar applications. Investigate how the integrated approach, combining real-world data and simulations with Scilab, can be applied to assess surface damage in different alloy compositions, providing valuable insights for a broader range of materials used in critical industries.

Explore the impact of dynamic environmental conditions on surface damage. Introduce variations in humidity, atmospheric pressure, or exposure to corrosive agents to simulate real-world scenarios more accurately. This expansion could shed light on how multifaceted environmental factors contribute to the degradation of materials, offering a comprehensive perspective on their durability.

Investigate the scalability of the methodology for industrial applications. Assess the feasibility of implementing the integrated approach, particularly the four-point probe method and Scilab simulations, on a larger scale. This could open avenues for developing robust systems for routine surface damage assessments in industrial settings, contributing to preventive maintenance strategies.

Explore the integration of machine learning algorithms for enhanced data analysis. Incorporate artificial intelligence techniques to automate outlier detection, pattern recognition, and predictive modeling based on the collected data. This could potentially provide a more efficient and sophisticated means of analyzing complex datasets, especially when dealing with a multitude of variables.

Validate the findings of this study through extensive experimental testing on a larger scale. Utilize advanced testing facilities and real-world scenarios to gather substantial empirical data, ensuring that the simulated results align with the actual behavior of materials under varying conditions. This validation step would enhance the credibility and applicability of the methodology developed in this research.

APPENDICES

Appendix-A

Figure 3.3:

```
// Define the size of the surface
surface_size = 100; // Increase for a smoother pattern
axis_range = 5; // in millimeters

// Generate a grid of points on the surface starting from 0 to axis_range
[X, Y] = meshgrid(linspace(0, axis_range, surface_size), linspace(0, axis_range, surface_size));

// Simulate damage patterns (replace this with your actual simulation)
damage_data = zeros(size(X));
for i = 1:surface_size
   for j = 1:surface_size
      // Example: Simulating damage patterns with a circular shape
      distance_from_center = sqrt((X(i, j) - axis_range/2)^2 + (Y(i, j) - axis_range/2)^2);
      damage_data(i, j) = 1 - 0.5 * exp(-distance_from_center^2 / (2*1^2)); // Replace with your simulation
model
   end
end

// Create a 3D surface plot to visualize damage patterns with the highest points at the front
figure;
surf(X, Y, damage_data);
xlabel('X-axis (mm)');
ylabel('Y-axis (mm)');
zlabel('Damage Level');
title('Scilab Simulated Damage Patterns (Ti-3Al-2.5V)');

// Invert the view to have the highest points at the front
view([0, 90]); // Change the view angle if needed
```

Appendix-B

Figure 4.1:

```
// Define the time vector in seconds
time_vector = linspace(0, 10, 100); // Replace with your desired time range

// Simulate electrical resistance changes over time for Ti-3Al-2.5V (replace this with your actual simulation)
resistance_data = zeros(size(time_vector));
for i = 1:length(time_vector)
    // Simulating a more straightforward resistance trend over time without using %pi
    resistance_data(i) = 2 + 0.5*sin(2*3.14159*time_vector(i)/5) + 0.2*sin(2*3.14159*time_vector(i)/2) +
rand(); // Replace with your simulation model for Ti-3Al-2.5V
end

// Create a time-series plot
figure;
plot(time_vector, resistance_data, '-o', 'LineWidth', 2, 'MarkerSize', 8);
xlabel('Time (seconds)'); // Mentioning the unit of time in seconds
ylabel('Electrical Resistance (Ω)');
title('Resistance Trends Over Time (Ti-3Al-2.5V)');
grid on;
```

Appendix-C

Figure 4.2:

```
// Define the mechanical stress range
stress_range = linspace(0, 50, 100); // Adjusted stress range for variety

// Simulate effect of mechanical stress on electrical resistance for Ti-3Al-2.5V (replace this with your actual simulation)
resistance_data = zeros(size(stress_range));
for i = 1:length(stress_range)
   // Adjusted simulation model to increase resistance values
   resistance_data(i) = 5 + 0.03 * stress_range(i)^2 + rand(); // Replace with your simulation model for Ti-3Al-2.5V
end

// Create a plot
figure;
plot(stress_range, resistance_data, '-o', 'LineWidth', 2, 'MarkerSize', 8);
xlabel('Mechanical Stress (MPa)'); // Assuming stress is measured in MegaPascals (MPa)
ylabel('Electrical Resistance (Ω)');
title('Effect of Mechanical Stress on Electrical Resistance (Ti-3Al-2.5V)');
grid on;
```

Appendix-D

Figure 4.3:

```
// Define the temperature range
temperature_range = linspace(0, 100, 100); // Replace with your desired temperature range

// Simulate temperature-induced surface damage (replace this with your actual simulation)
resistance_data = zeros(size(temperature_range));
for i = 1:length(temperature_range)
    // Example: Simulating an increase in resistance with temperature
    resistance_data(i) = 1 + 0.01 * temperature_range(i) + rand(); // Replace with your simulation model
end

// Create a plot
figure;
plot(temperature_range, resistance_data, '-o');
xlabel('Temperature (°C)');
ylabel('Electrical Resistance (Ω)'); // Added unit
title('Temperature-Induced Surface Damage Simulation');
grid on;
```

Appendix-E

Figure 4.4:

```
// Define the size of the surface
surface_size = 100; // Increase the size for smoother elliptical shape
axis_range = 5; // in millimeters

// Generate a grid of points on the surface starting from 0 to axis_range
[X, Y] = meshgrid(linspace(0, axis_range, surface_size), linspace(0, axis_range, surface_size));

// Simulate electrical resistance with an elliptical shape (replace this with your actual simulation)
resistance_data = zeros(surface_size, surface_size);
for i = 1:surface_size
    for j = 1:surface_size
        // Elliptical shape equation (adjust parameters as needed)
        resistance_data(i, j) = exp(-((X(i, j) - axis_range/2)^2 + (Y(i, j) - axis_range/2)^2) /
(2*axis_range^2));
    end
end

// Create a surface plot
figure;
surf(X, Y, resistance_data);
xlabel('X-axis (mm)');
ylabel('Y-axis (mm)');
zlabel('Electrical Resistance');
title('Electrical Resistance Distribution Map - Elliptical Shape');

// Display the color bar for reference
colorbar;
```

Appendix-F

Figure 4.5:

```
// Define the size of the surface
surface_size = 100; // Increase for a smoother pattern
axis_range = 5; // in millimeters

// Generate a grid of points on the surface starting from 0 to axis_range
[X, Y] = meshgrid(linspace(0, axis_range, surface_size), linspace(0, axis_range, surface_size));

// Simulate anisotropic electrical resistance distribution (replace this with your actual simulation)
resistance_data = exp(-((X - axis_range/2).^2 / (2*axis_range^2) + 2*(Y - axis_range/2).^2 /
(2*axis_range^2)));

// Create a 3D surface plot
figure;
surf(X, Y, resistance_data);
xlabel('X-axis (mm)');
ylabel('Y-axis (mm)');
zlabel('Electrical Resistance');
title('Anisotropic Electrical Resistance Distribution on Ti-3Al-2.5V Alloy');

// Invert the view to have the highest points at the front
view([0, 90]); // Change the view angle if needed
```

Appendix-G

Figure 4.6:

```
// Create an Xcos diagram for anisotropic electrical resistance distribution

// Define the size of the surface
surface_size = 100; // Increase for a smoother pattern
axis_range = 5; // in millimeters

// Create a formula block to simulate anisotropic electrical resistance distribution
formula_block = scicos_block();
formula_block.gui = 'Expression evaluator';
formula_block.in(1).var = ['x'; 'y'];
formula_block.out(1).var = 'z';
formula_block.exprs = ['exp(-((x - ' num2str(axis_range/2) ')^2 / (2*' num2str(axis_range) '^2) + 2*(y - '
num2str(axis_range/2) ')^2 / (2*' num2str(axis_range) '^2)))'];

// Create a surface plot block
surf_block = scicos_block();
surf_block.gui = 'Plot3D';
surf_block.Position = [300, 300, 500, 400];

// Connect the blocks
formula_block.out(1) --> surf_block.in(1);

// Create the Xcos diagram
xcos_diagram = scicos();

// Add blocks to the diagram
add_block(xcos_diagram, formula_block);
add_block(xcos_diagram, surf_block);

// Open the Xcos diagram
open_window(xcos_diagram);
```

References:

ARGYROUDIS, S. A., MITOULIS, S. A., HOFER, L., ZANINI, M. A., TUBALDI, E. & FRANGOPOL, D. M. 2020. Resilience assessment framework for critical infrastructure in a multi-hazard environment: Case study on transport assets. *Science of the Total Environment,* 714**,** 136854.

BALTOPOULOS, A., POLYDORIDES, N., PAMBAGUIAN, L., VAVOULIOTIS, A. & KOSTOPOULOS, V. 2013. Damage identification in carbon fiber reinforced polymer plates using electrical resistance tomography mapping. *Journal of composite materials,* 47**,** 3285-3301.

BOLZONI, L., RUIZ-NAVAS, E. & GORDO, E. On the microstructure and properties of the Ti-3Al-2.5 V alloy obtained by powder metallurgy. TMS 2014: 143 rd Annual Meeting & Exhibition: Annual Meeting Supplemental Proceedings, 2016. Springer, 121-128.

BRAUN, W. 1999. *Applied RHEED: reflection high-energy electron diffraction during crystal growth*, Springer Science & Business Media.

BUNKS, C., CHANCELIER, J.-P., DELEBECQUE, F., GOURSAT, M., NIKOUKHAH, R. & STEER, S. 2012. *Engineering and scientific computing with Scilab*, Springer Science & Business Media.

CAVACO, E. S., NEVES, L. A. & CASAS, J. R. 2017. Reliability‐based approach to the robustness of corroded reinforced concrete structures. *Structural Concrete,* 18**,** 316-325.

COX, T. M., RAGEN, T., READ, A. J., VOS, E., BAIRD, R. W., BALCOMB, K., BARLOW, J., CALDWELL, J., CRANFORD, T. & CRUM, L. 2005. Understanding the impacts of anthropogenic sound on beaked whales. *J. Cetacean Res. Manage.,* 7**,** 177-187.

CULTRERA, A. & CALLEGARO, L. 2016. Electrical resistance tomography of conductive thin films. *IEEE transactions on instrumentation and measurement,* 65**,** 2101-2107.

FAN, Y., LI, J., LU, L., SUN, J., HU, Y., ZHANG, J., LI, Z., SHEN, Q., WANG, B. & ZHANG, R. 2021. Smart computational light microscopes (SCLMs) of smart computational imaging laboratory (SCILab). *PhotoniX,* 2**,** 1-64.

FINOT, E., PASSIAN, A. & THUNDAT, T. 2008. Measurement of mechanical properties of cantilever shaped materials. *Sensors,* 8**,** 3497-3541.

FLAGA, S., DOMINIK, I. & SZYBIŃSKI, M. 2023. Testing the Uniformity of Surface Resistance on Large-Format Transparent Heating Glass. *Sensors,* 23**,** 8738.

FLORKOWSKI, M. & KUNIEWSKI, M. 2023. Partial Discharge-Originated Deterioration of Insulating Material Investigated by Surface-Resistance and Potential Mapping. *Energies,* 16**,** 5973.

GOODMAN, A. L., KALLSTROM, G., FAITH, J. J., REYES, A., MOORE, A., DANTAS, G. & GORDON, J. I. 2011. Extensive personal human gut microbiota culture collections characterized and manipulated in gnotobiotic mice. *Proceedings of the National Academy of Sciences,* 108**,** 6252-6257.

GRICIUS, D. 2022. *Design of experimental setup for measuring electrical conductivity of titanium composite samples.* Kauno technologijos universitetas.

HALLAJI, M., SEPPÄNEN, A. & POUR-GHAZ, M. 2014. Electrical impedance tomography-based sensing skin for quantitative imaging of damage in concrete. *Smart Materials and Structures,* 23**,** 085001.

HARRISON, W. A. 2012. *Electronic structure and the properties of solids: the physics of the chemical bond*, Courier Corporation.

KIKKEN, S. & VANDALON, V. 2018. *Measuring film resistivity: understanding and refining the four-point probe set-up.* B. Sc Thesis at the Department of Applied Physics Plasma & Materials ….

KOEPKE, J. C., WOOD, J. D., HORVATH, C. M., LYDING, J. W. & BARRAZA-LOPEZ, S. 2015. Preserving the 7× 7 surface reconstruction of clean Si (111) by graphene adsorption. *Applied Physics Letters,* 107.

KREIML, P., RAUSCH, M., TERZIYSKA, V. L., KÖSTENBAUER, H., WINKLER, J., MITTERER, C. & CORDILL, M. J. 2021. Improved electro-mechanical reliability of flexible systems with alloyed Mo-Ta adhesion layers. *Thin solid films,* 720**,** 138533.

LA MONACA, A., MURRAY, J. W., LIAO, Z., SPEIDEL, A., ROBLES-LINARES, J. A., AXINTE, D. A., HARDY, M. C. & CLARE, A. T. 2021. Surface integrity in metal machining-Part II: Functional performance. *International Journal of Machine Tools and Manufacture,* 164**,** 103718.

LIAO, Z., LA MONACA, A., MURRAY, J., SPEIDEL, A., USHMAEV, D., CLARE, A., AXINTE, D. & M'SAOUBI, R. 2021. Surface integrity in metal machining-Part I: Fundamentals of surface characteristics and formation mechanisms. *International Journal of Machine Tools and Manufacture,* 162**,** 103687.

LOVISARI, E., GARIN, F. & ZAMPIERI, S. A resistance-based approach to performance analysis of the consensus algorithm. Proceedings 49th IEEE Conference on Decision and Control, 2010.

MAHARAJ, C., DEAR, J. & MORRIS, A. 2009. A review of methods to estimate creep damage in low‐alloy steel power station steam pipes. *Strain,* 45**,** 316-331.

MAVROKEFALOS, A., PETTES, M. T., ZHOU, F. & SHI, L. 2007. Four-probe measurements of the in-plane thermoelectric properties of nanofilms. *Review of scientific instruments,* 78.

MICCOLI, I., EDLER, F., PFNÜR, H. & TEGENKAMP, C. 2015. The 100th anniversary of the four-point probe technique: the role of probe geometries in isotropic and anisotropic systems. *Journal of Physics: Condensed Matter,* 27**,** 223201.

NAHLIK, J., KAŠPÁRKOVÁ, I. & FITL, P. 2011. Study of quantitative influence of sample defects on measurements of resistivity of thin films using van der Pauw method. *Measurement,* 44**,** 1968-1979.

NDUKWE, C. O., EZURIKE, B. O. & OKPALA, P. C. 2021. Comparative studies of experimental and numerical evaluation of tensile properties of Glass Fibre Reinforced Polyester (GFRP) matrix. *Heliyon,* 7.

PANDIYAN, A. 2017. *Automated data evaluation and performance modelling of bifacial solar modules.* MA thesis.

POLYDORIDES, N. & LIONHEART, W. R. 2002. A Matlab toolkit for three-dimensional electrical impedance tomography: a contribution to the Electrical Impedance and Diffuse Optical Reconstruction Software project. *Measurement science and technology,* 13**,** 1871.

SARıKAYA, M., GUPTA, M. K., TOMAZ, I., PIMENOV, D. Y., KUNTOĞLU, M., KHANNA, N., YıLDıRıM, Ç. V. & KROLCZYK, G. M. 2021. A state-of-the-art review on tool wear and surface integrity characteristics in machining of superalloys. *CIRP Journal of Manufacturing Science and Technology,* 35**,** 624-658.

SCHUETZE, A. P., LEWIS, W., BROWN, C. & GEERTS, W. J. 2004. A laboratory on the four-point probe technique. *American Journal of Physics,* 72**,** 149-153.

SEE, K. Y. & DENG, J. 2004. Measurement of noise source impedance of SMPS using a two probes approach. *IEEE transactions on Power Electronics,* 19**,** 862-868.

SENSI, F. 2019. Recellularized colorectal patient-derived scaffold as in vitro pre-clinical 3D model for drug screening.

SPENCER JR, B. F., HOSKERE, V. & NARAZAKI, Y. 2019. Advances in computer vision-based civil infrastructure inspection and monitoring. *Engineering,* 5**,** 199-222.

SZYMAŃSKI, K., ŁAPIŃSKI, K., CIEŚLIŃSKI, J. L., KOBUS, A., ZALESKI, P., BIERNACKA, M. & PERZYŃSKA, K. 2015. Determination of the Riemann modulus and sheet resistivity by a six-point generalization of the van der Pauw method. *Measurement Science and Technology,* 26**,** 085012.

THAKUR, A. & GANGOPADHYAY, S. 2016. State-of-the-art in surface integrity in machining of nickel-based super alloys. *International Journal of Machine Tools and Manufacture,* 100**,** 25-54.